

CHAPTER 1

CURRENT STATUS OF INTRASEASONAL-SEASONAL-TO-INTERANNUAL PREDICTION OF THE INDO-PACIFIC CLIMATE

Jing-Jia Luo^{1,2}, June-Yi Lee³, Chaoxia Yuan², Wataru Sasaki², Sebastien Masson⁴, Swadhin K. Behera², Yukio Masumoto², and Toshio Yamagata²

¹*Centre for Australian Weather and Climate Research, Bureau of Meteorology, Melbourne, Australia*

²*Research Center for Global Change/Application Laboratory, Japan Agency for Marine Earth Science and Technology, Yokohama, Japan*

³*Institute of Environmental Studies, Pusan National University, Busan, Korea*

⁴*LOCEAN/IPSL, CNRS/IRD/UPMC/MNHN, Universite Pierre et Marie Curie, Paris, France*

Prediction skill of the Indo-Pacific climate has been rapidly enhanced in the past decades. While early prediction efforts were made based on statistical methods and/or simple climate models, recent climate predictions have been performed using comprehensive ocean-atmosphere general circulation models (OAGCMs). Both model performance of climate simulation and data assimilation scheme have been improved to produce better prediction skill. Multi-model prediction results have been collected to gain higher skill, which is usually superior to that of individual model. Most of OAGCMs now can skilfully predict Indian Ocean Dipole (IOD) at lead times of up to 1-2 seasons, and ENSO up to 6-9 months. Distinct SST patterns associated with different El Niño flavours can also be well predicted at short-mid lead times. Furthermore, global climate anomalies induced by ENSO and IOD are realistically predicted. The subtropical dipole modes in the South Atlantic and Indian Ocean (IO), the southern African climate, Asian monsoon precipitation, and Northern Hemisphere atmospheric circulation anomalies are predictable at short-mid lead times. Encouragingly, the JAMSTEC SINTEX-F model produces useful skill of ENSO prediction at lead times of up to 2-year. And some strong IOD events can be well predicted up to 1 year ahead even if El Niño's influence were suppressed. The results also suggest the importance of IO-Pacific inter-basin coupling and recent global warming trend to the climate predictability. For MJO prediction, multi-model ensemble based on 12 OAGCMs achieves useful skill (>0.5) up to 26-28 days in advance.

1. Introduction

The Earth's climate varies significantly at broad frequencies, covering monthly, intraseasonal, seasonal, annual, interannual, decadal, multidecadal, centennial and longer time scales. The climate anomalies bring warm or cold, dry or wet weather events, and sometimes disasters like severe flooding, drought, storms, heat waves, cold surges and

so on. Severe climate events may trigger crisis of water, food, and energy supply, environmental problems, socio-economic losses, and even conflicts (wars) between different countries and nations (Hsiang et al. 2011). It is found that the frequency of climate extremes may likely have increased over past decades and would likely keep increasing under global warming (IPCC AR5 report,

<http://climatechange2013.org/>). Similarly, variations in ocean, often driven by surface winds and buoyancy fluxes, may considerably affect the oceanic biological processes and hence fisheries worldwide. Therefore, the climate anomalies could exert tremendous environmental and socio-economic influence over the globe. There has been a high demand for useful forecast of climate anomalies at lead times that are sufficiently ahead of decision making horizon.

Predictability of the earth's climate can be categorized into two types: one rooted in the initial value and the other in the boundary forcing (Lorenz 1975). A well-known example for predictability of the first type is weather forecast. Given a perfect atmospheric model, predictability of weather is essentially determined by the accuracy of atmospheric initial conditions (ICs) (if intrinsic model errors can be ignored). It is found that predictability of tropical intraseasonal oscillations is also largely determined by the atmospheric ICs though air-sea coupling processes have influences on MJO propagation (Sperber et al. 2005). Projection of climate change from 30 years to one century, an example of the second type of predictability, is to assess how the earth's climate would change under the radiative forcing of increasing greenhouse gases (GHGs) and other anthropogenic and natural agents (IPCC AR4 report, <http://www.ipcc.ch/>). For decadal climate predictions, both ICs (mainly of slow-varying components like ocean) and the external radiative forcing are important, as suggested by recent studies (IPCC AR5 report, <http://climatechange2013.org/>). On seasonal-to-interannual time scales, climate predictability primarily originates from the ocean-atmosphere coupled variability in the

tropics, where the ocean provides a key memory and lower boundary forcing of the atmosphere. The tropical climate signals can be predicted at lead times of several months to seasons and even up to 1–2 years based on current state-of-the-art fully coupled models (e.g., Palmer et al. 2004; Luo et al. 2007, 2008b; Jin et al. 2008; Wang et al. 2009; Barnston et al. 2012; Wang et al. 2010). It is believed that a modest predictability of global climate anomalies can be gained owing to significant impacts of the predictable tropical signals, particularly El Niño–Southern Oscillation (ENSO) and Indian Ocean Dipole (IOD) events.

It is widely recognized that the tropical upper ocean memory has a major contribution to the seasonal and interannual climate predictability. The dynamical oceanic processes, such as the Rossby and Kelvin wave propagations and associated basin-wide ocean adjustment or subsurface temperature anomalies, can trigger tropical climate anomalies which rapidly grow via vigorous ocean-atmosphere interactions and hence provide key precursors for the climate prediction (e.g., Luo 2011). Understanding the tropical climate (particularly ENSO) dynamics has provided the basis for the development of climate prediction systems over the past decades. Additional but minor sources of climate predictability include other tropospheric lower or upper boundary forcing such as soil moisture, sea ice, snow cover, vegetation, stratospheric conditions (e.g., Sigmond et al. 2013), and atmospheric modes such as Madden-Julian Oscillation (MJO), Southern Annular Mode, Arctic Oscillation, North Atlantic Oscillation, and Quasi-Biennial Oscillation. In general, predictability of these low-frequency atmospheric modes is limited at

lead times of up to a few weeks; some of their predictability is partly attributed to the remote influence of tropical climate. It is still unclear how much those less-important boundary conditions can contribute to the climate predictability. For example, it is found that soil moisture deficit has impacts on hot extremes in southeast Europe (Hirschi et al. 2010), and realistic land surface condition may improve the potential predictability of precipitation over semiarid regions (Kanae et al. 2006). Preliminary prediction results however suggest that their impacts may be mostly limited to subseasonal time scale, local areas, specific seasons or circumstances (Koster et al. 2010; see the review article of Stockdale et al. 2010).

External radiative forcing may also play a role in seasonal-to-interannual climate predictability. The natural solar radiation varies at a notable period of 11 years; its variation, despite small relative to its mean value, may generate climate anomalies for example in the tropical Pacific (Meehl et al. 2009). Large volcanic eruptions, particularly in the tropical area, may occasionally generate visible impacts on the global-mean climate and sea level height (Robock et al 2000; Church 2005), although the volcano-induced signals are generally small compared to natural climate variability at seasonal-to-interannual timescales. The time-variation of solar radiation and volcanic eruptions has been usually neglected in climate prediction models but are required to be introduced in next-generation of forecast systems. The increasing anthropogenic emissions of GHGs and other agents in past decades have contributed to the long-term rise of global mean land surface temperature and upper ocean heat storage (Levitus et al. 2000). Since the human-induced global warming signal has been partly

incorporated into the ICs of a climate prediction system and GHGs concentrations usually do not change much within the forecast period (i.e., several months to 1-2 years), concentrations of GHGs have been usually fixed at present-day levels in atmospheric models. Recent studies, however, suggested that better capturing the global warming trend during forecast may improve climate prediction particularly at long-lead times (see section 5).

Climate predictions are usually performed by means of simple statistical models or comprehensive dynamical numerical models or the combination of the two. Statistical models are cheap and often built based on a linear or nonlinear relation between a set of factors (i.e. predictor) and phenomena to be predicted (i.e. predictand). The relation can be obtained from a theoretical basis of dynamical understanding or pure statistical relation. Often used statistical methods include persistence (Knaff and Landsea 1997), analogue analysis (van den Dool et al. 2003), linear multiple regression (McPhaden et al. 2006; Izumo et al. 2010 and 2014), linear Markov process (Xue et al. 2000), linear inverse model (Penland and Matrosova 1998), canonical correlation analysis (Barnston and Ropelewski 1992), nonlinear neural network (Wu et al. 2006), etc. Statistical predictions are conducted by assuming that statistical relations built from historically observations are expected to apply in the future. This assumption, however, may become invalid under circumstances when the statistical relations between predictors and predictands vary with time due to either natural processes or anthropogenic forcing. Other obvious drawbacks of statistical models include over-fitting and outlier problem. To reduce artificial skill which arises from over-fitting, leave-one-

out cross validation (i.e., using a single observation from the original sample as the validation data, and the remaining observations as the training data) is often adopted. Statistical models are known to have difficulty in dealing with unprecedented events and nonlinear relations in the climate system. Despite these caveats, statistical models are capable to produce comparable skill in predicting climate signals compared to dynamical models (Barnston et al. 1999).^a One advantage over dynamical models is that statistical models are able to downscale climate information into a regional scale which dynamical models have limits to reach. Another advantage is that statistical models have much less bias because they are trained based on observational data. Statistical models are also widely used to apply weather/climate predictions into various social-economical activities, including agriculture, water manage, energy saving, fishery, tourism, etc. So far, a hierarchy of statistical prediction models has been developed and are continued to be improved for climate forecast and its societal application.

Sophisticated ocean-atmosphere coupled general circulation models (GCMs) should be able to handle unprecedented climate signals and their dynamically linked teleconnections over the globe. For dynamical model prediction, two general approaches are often adopted to assess climate predictability. One is for potential predictability assessment by assuming both model and ICs are perfect. While this method is useful for assessing the upper limit of climate predictability, the estimated predictability may be considerably

influenced by model errors. The other approach is for practical predictability assessment by measuring model ability in forecasting the observed climate from as realistic as possible ICs.

The practical forecasts are performed with two different strategies: two-tiered and one-tiered techniques. In the two-tiered method, sea surface temperature (SST) anomaly, particularly in the tropics, is first predicted based on a simple ocean-atmosphere coupled model (usually with fixed climatology as observed). And the predicted SST anomaly is added into observed SST climatology to force atmosphere GCMs with complex physics (Bengtsson et al. 1993). This method was often used in early stage owing to the poor performance of fully coupled models in simulating/predicting climate. Because SST is not always a forcing of atmosphere but a result of atmospheric forcing under some circumstances, particularly in monsoon areas and mid-high latitudes (Wang et al. 2005), the two-tiered method might lead to intrinsic errors in simulating/predicting atmospheric anomalies outside the tropics. To overcome the fully coupled models' errors, an intermediate way was developed by applying flux corrections into OAGCMs to maintain realistic climatology. The anomaly coupling and flux corrections were widely used in the first generation of models for climate prediction (e.g., Ji et al. 1996; Cane et al. 1986). The flux corrections, however, may introduce unrealistic physical processes (Dijkstra et al. 1995), hamper the air-sea interactions and hence weaken predictive climate signals. Increasing efforts have been made over the past 1-2 decades on developing fully coupled OAGCMs without any flux adjustment. It is encouraging that skill of the

^a We note that prediction results in recent decade suggest that dynamical OAGCMs have encouragingly outperformed statistical models particularly for ENSO phase transition prediction (e.g., Barnston et al. 2012).

Table 1: List of current major operational seasonal forecast systems. Note that APEC Climate Center issues multi-model predictions by collecting the forecasts from other operational centers

Forecast system	Atmosphere component	Ensemble size	Lead month	Re-forecast period	Initialization scheme
	Ocean component				
ECMWF System4 (Molteni et al. 2011)	IFS cycle 36r4, T255L91	51	7	1981-present	ECMWF operational analysis NEMOVAR ocean reanalysis
	NEMO, ORCA1				
NCEP CFSv2 (Saha et al. 2010)	T126L64	40	9	1982-present	NCEP Climate Forecast System Reanalysis.
	MOM4, 0.5°×0.25°~0.5°×40 levels				
UK Met Office GloSea4 (Arribas et al. 2011)	Met Office Unified Model, N96L38	42	7	1989-present	Met Office operational analysis; Ocean data assimilation
	NEMO, ORCA1				
BOM POAMA2 (http://poama.bom.gov.au/)	BAM3.0, T47L17	99	9	1981-present	Atmosphere-Land Initialization Scheme; POAMA Ensemble Ocean Data Assimilation System
	ACOM2, 2°×0.5°~1.5°×25 levels				
JMA MRI-CGCM (http://ds.data.jma.go.jp/tcc/tcc/products/elnino/jmamri_cgcm_doc.html)	JMA-GSM (JMA 2007), T95L40	51	15	1979-present	JMA operational analysis; Ocean data assimilation
	MRI.COM, 1°×0.3°~1°×50 levels				
JAMSTEC SINTEX-F (Luo et al. 2005b)	ECHAM4, T106L19	27	24	1982-present	Coupled SST-nudging initialization
	OPA8, ORCA2				

one-tiered method (which predicts the climate signals using the fully coupled OAGCMs directly) in predicting atmospheric anomalies has now beaten that of the two-tiered method.

It has been realized that skilful predictions require good performance of coupled models in simulating major climate modes such as ENSO and IOD, in particular, their periods, amplitudes, spatial structures, and phase relationships with the annual cycle (e.g., Luo

et al. 2008a; Lee et al. 2010, 2011; Jia et al. 2012; Wang et al. 2014). It is also important to resolve the associated teleconnection patterns and to retain model's climatology close to observations. Besides, the ICs used for forecasts should be not only realistic but also compatible between the ocean and atmosphere. In addition, a good ensemble scheme should be designed to reflect the uncertainties in both ICs and model physics.

Early generations of fully coupled models often produced too frequent ENSO events and their related SST anomalies were confined too much toward the equator. Although the spurious semi-annual cycle of SST in the eastern equatorial Pacific has been improved in the latest generation of OAGCMs (i.e. CMIP5 models), the exaggerated equatorial cold tongue and double ITCZ bias in the tropical Pacific have yet to be solved. In the tropical Indian Ocean (IO), many models still produce too strong IOD variability in association with too weak mean westerly (or erroneous easterly) along the equator and hence too shallow thermocline in the eastern Indian Ocean (EIO).

Oceanic and atmospheric ICs are often separately generated in climate prediction systems. Recent efforts have been made on coupled model initialization to produce ocean-atmosphere balanced ICs for reducing initial shocks during forecast (Chen et al. 2004; Keenlyside et al. 2005; Luo et al. 2005b). Good strategies for generating initial perturbations are required to produce sufficient spreads during forecast. However, many forecast systems based on a single OAGCM are often found to be over-confident. That is, their ensemble spreads are smaller than prediction errors, or in other words, too narrow to represent the range of observed outcomes. It turns out that multi-model approach or perturbing model physics helps reduce the over-confidence problem despite the caveat that the multi-model ensembles may have common errors. Real time ensemble forecasts have now been issued at several operational centers (Table 1).

While classic theories for the tropical climate tell us that climate anomalies (like ENSO and IOD) can be predicted

deterministically if the subsurface signals (or other long-memory precursors) are known, the climate predictions are of probabilistic nature (Kumar and Murtugudde 2013). This is particularly true in the extratropics where atmosphere is less influenced by SST and atmosphere itself has strong internal variability which is mostly unpredictable at seasonal and longer time scales. Because of the different nature of the tropical and extratropical climate, predictability of the tropical climate is often measured by means of deterministic skill, including the simple anomaly correlation coefficient (ACC), root mean square error (RMSE), and mean square skill score. Whereas, for the extra-tropical areas with modest predictability, probabilistic prediction skill is a more appropriate measure, including the Brier skill score and the relative operating characteristic curve score. We note that ENSO prediction is now also issued in a probabilistic way. While the phase transition from El Niño to La Niña is often predictable, prediction of El Niño onset is occasionally difficult since intraseasonal disturbances including westerly wind bursts in the western equatorial Pacific may play an important role in triggering and affecting the development of El Niño events (e.g., McPhaden 1999). In the tropical IO where strong intraseasonal oscillations often develop (and hence signal-to-noise ratio is low) and where local ocean-atmosphere coupling is not strong, IOD predictability is low compared to ENSO predictability.

Figure 1 shows the ACC skill of global SST anomaly for the period 1982-2012 based on JAMSTEC SINTEX-F climate prediction system (detailed information are given in section 2, see Luo et al. 2005b, 2007, 2008b). The retrospective prediction results indicate

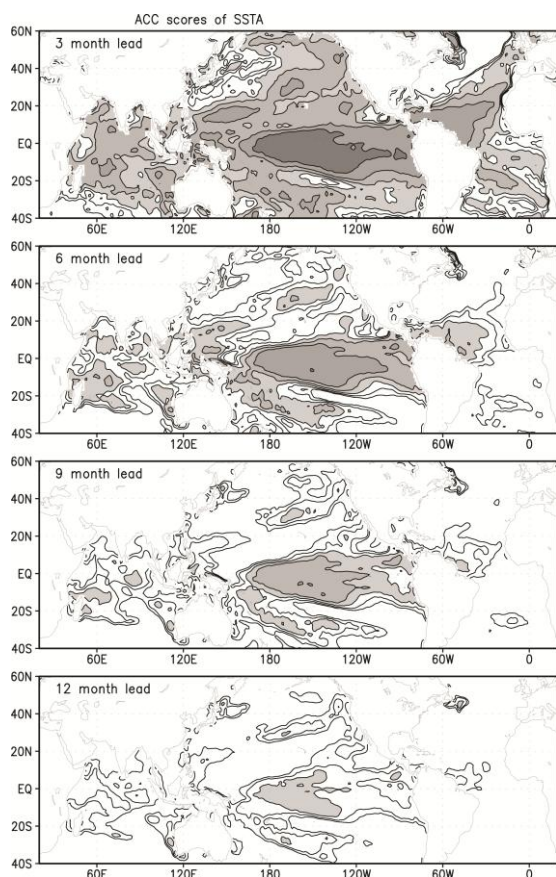


Figure 1: SST anomaly correlations between the NCEP observations and SINTEX-F model nine-member ensemble mean predictions at 3-, 6-, 9-, and 12-month lead times for the period 1982–2012. Contour interval is 0.1 and regions with values above 0.6 (below 0.4) are shaded (not shown). Skills are calculated based on the time series of a 5-month running mean of both the observations and model predictions at each lead time. When calculating model forecast anomalies, model climate drifts have been removed at each lead time in *a posteriori* manner (see Luo et al. 2005b, 2008a).

high predictability (>0.6) in the tropical Pacific up to 1-year lead and up to 6–9 months lead in many parts of tropical IO, particularly in the eastern equatorial IO, southwestern IO and west of Australia. Prediction skill is also relatively high up to 6–9 months ahead in the North and South Pacific associated with

ENSO teleconnections. Compared to the other two basins, climate prediction in the Atlantic is the most challenging which is common to existing forecast systems (Stockdale et al. 2006). While the tropical western Atlantic shows high prediction skill up to 6–9 months lead mostly due to ENSO remote influence (Luo et al. 2005b), limited skill is seen in the equatorial eastern Atlantic even at 3-month lead. One primary reason for this is that most of current coupled models fail to reproduce the climatological west warm-east cold structure along the equatorial Atlantic (e.g., Luo et al. 2005a).

In this chapter, we shall focus on the climate prediction in the Indo-Pacific region based on fully coupled OAGCMs. Skill assessment presented here is given in a deterministic manner for simplicity. ENSO predictions based on multi-model ensembles up to 6-month ahead and a single model up to 2-year ahead as well as prediction of two types of ENSO are introduced in section 2. Section 3 presents the climate prediction in the IO, including IOD, basin wide mode, and SST variability in the southwestern IO and west of Australia. ENSO-IOD interactions are also briefly discussed. In section 4, extratropical climate prediction, particularly the subtropical dipole modes in the IO and Atlantic and southern African climate, is presented. Impact of recent global warming on seasonal-to-interannual prediction is discussed in section 5. Section 6 is devoted to MJO prediction which is important to build a seamless climate prediction system. Summary and discussions of current status and future development of climate prediction are given in section 7.

2. ENSO prediction

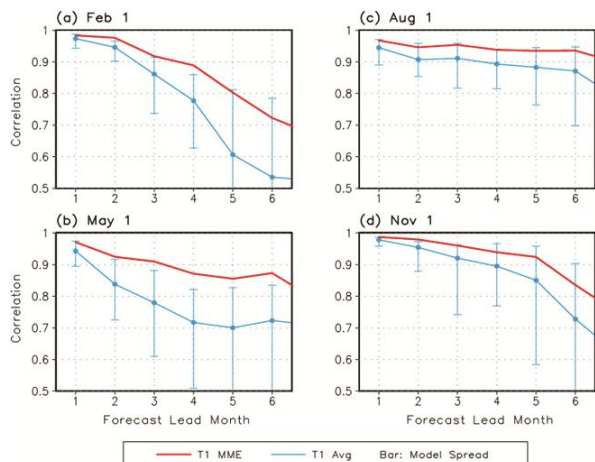


Figure 2.1: ACC skill for the Nino3.4 SST index (5°S – 5°N , 170°W – 120°W) as a function of forecast lead time, initiated from (a) February 1, (b) May 1, (c) August 1, and (d) November 1 for the period of 1981–2001 derived from 14 coupled models that participated in CliPAS and DEMETER projects. The mid-blue lines indicate the averaged skill of the individual models and the bars show the range of the best and worst coupled model skills. The red lines denote the multi-model ensemble (MME) mean prediction skill based on the 14 coupled models.

ENSO in the tropical Pacific is the most dominant driver for year-to-year climate variability on Earth. The prediction of ENSO and its related climate impacts sufficiently ahead of its onset is vital for effective management of climate disasters over the globe. Following the first successful forecast of the 1986/87 El Niño event with a simple coupled model (Cane et al. 1986), significant progress in the ENSO prediction has been achieved using OAGCMs. Real time ENSO forecasts based on either dynamical or statistical models have now been issued on a monthly basis at many operational centers and research institutions (e.g., <http://iri.columbia.edu/climate/ENSO/index.ht>

[ml](#); Graham et al. 2011). In theory, ENSO is believed to be predictable on the order of one or two years in advance owing to the self-sustained nature of the tropical Pacific coupled ocean-atmosphere system (e.g., Neelin et al. 1998). However, a majority of existing forecast systems exhibited useful prediction skill of ENSO over the past 2–3 decades up to only two or three seasons ahead (e.g., Barnston et al. 1999; Palmer et al. 2004; Jin et al. 2008; Xue et al. 2011).

2.1. Multi-model prediction of ENSO up to 6 months lead

Fig. 2.1 shows ACC skill for the Nino 3.4 SST anomaly averaged over the region (5°S – 5°N , 170°W – 120°W) as a function of forecast lead time for the period of 1981–2001 derived from 13 coupled models (Table 2) that participated in CliPAS and DEMETER project. Readers are referred to Jin et al. (2008) and Wang et al. (2009) for detailed information on models and hindcast experiments. The results showed that ENSO can be predicted at 6-month lead with correlation skill of 0.86 using multi-model ensemble (MME) approach with the state-of-the-art coupled models. The MME’s ACC skill depends on the initial month from which the prediction is started. When the prediction starts from August 1st, the MME’s ACC skill for the Nino3.4 SST index reaches above 0.9 up to 6 months lead. Jin et al. (2008) further found that the forecast skill varies with season, ENSO phases, and ENSO intensity. A stronger El Niño or La Niña is more predictable than weak ENSO and neutral years.

2.2. Multi-model prediction of two types of ENSO at short lead times

Table 2: Description of the 13 coupled ocean-atmosphere models that participated in CliPAS and DEMETER project (see Jin et al. 2008 and Wang et al. 2009 for more detailed descriptions).

Institute	Model Name	AGCM	OGCM	Ensemble member
NCEP	CFS	GFS T62 L64	MOM3 1/3°lat x 5/8°lon L27	15
FRCGC	SINTEX-F	ECHAM4 T106L19	OPA 8.2 2° cos(lat)x2° lon L31	9
SNU	SNU	SNU T42L21	MOM2.2 1/3°lat x 1°lon L40	6
UH	UH	ECHAM4 T31L19	UH Ocean 1°lat x 2°lon L2	10
GFDL	CM2.1	AM2.1 2°lat x 2.5°lon L24	MOM4 1/3°lat x 1°lon L50	10
BMRC	POAMA1.5	BAM 3.0d T47 L17	ACOM3 0.5-1.5° lat x 2.0° lon L31	10
CERFACE	CERFACE	ARPEGE T63 L31	OPA 8.2 2.0° x2.0° L31	9
ECMWF	ECMWF	IFS T95 L40	HOPE-E 1.4° x 0.3°-1.4° L29	9
INGV	INGV	ECHAM4 T42 L19	OPA 8.2 2.0° lat x 2.0° lon L31	9
LODYC	LODYC	IFS T95 L40	OPA 8.0 182GPx152GP L31	9
MPI	MPI	ECHAM5 T42 L19	MPI-OM1 2.5° lat x 0.5°-2.5° lon L23	9
Meteo-France	Meteo-France	ARPEGE T63 L31	OPA 8.0 182GPx152GP L31	9
UKMO	UKMO	HadAM3 2.5x3.75L19	GloSea OGCM 1.25°x0.3-1.25°L40	9

El Niño was often referred to as a substantial SST warming in the equatorial eastern Pacific. Recent observations however showed that major warming of El Niño events during recent decades has frequently been confined in the central Pacific with less warming or even slight cooling in the east, which is called as Modoki (i.e., pseudo), central Pacific or

warm-pool El Niño. The different El Niño pattern was found to have distinct impacts on ecosystems, climate and hurricanes worldwide. For instance, compared to the eastern Pacific SST warming, the central Pacific warming could exert more severe drought in Australia and India. The changing El Niño has caused a new challenge not only for seasonal prediction

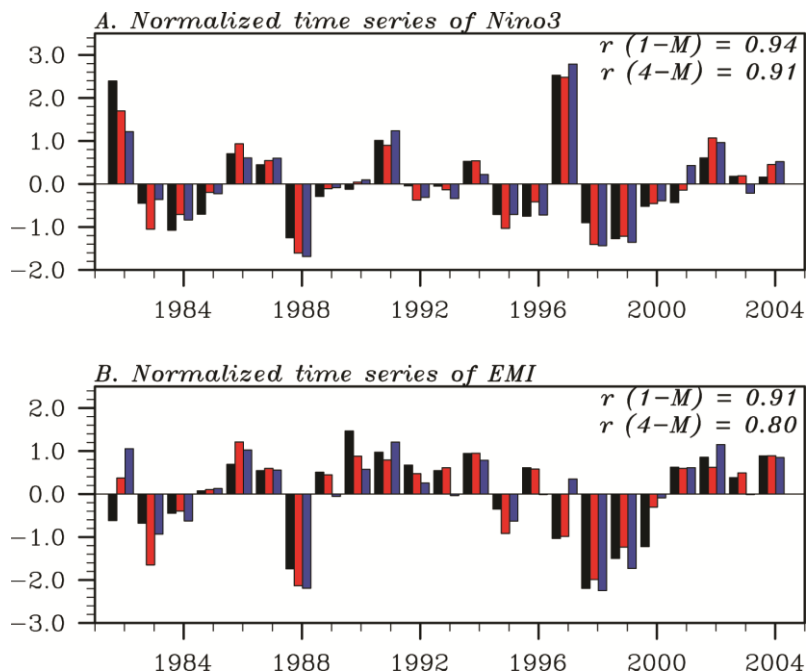


Figure 2.2: Normalized Dec-Jan-Feb mean anomalies of (a) Nino3 (5°S – 5°N , 150°W – 90°W) and (b) El Niño Modoki index based on observations (black bars) and MME mean predictions at 1 month (red bars) and 4 (blue bars) months lead time. Temporal correlations between the observed and MME predicted time series are given at the upper right (courtesy of Jeong et al. 2012).

of El Niño and its global impacts but also for projections of the 21st century climate change. Predictive skill of the SST warming in the central Pacific was found to be low in general but can be quite high under specific circumstances. For instance, the 1994/95 event has relatively low predictability (Luo et al. 2007). In contrast, the 2002/03 event is well predicted up to 2-year in advance (Luo et al. 2008b).

Prediction skill of the two types of ENSO was assessed based on five coupled OAGCMs collected at APEC Climate Center. The five model retrospective forecasts of the period 1982-2004 were provided by NCEP, Australian Bureau of Meteorology (BoM), JAMSTEC, Seoul National University, and APEC Climate Center. An ensemble mean of

each model (with the number of ensemble members varying from 5 to 15) is used to build a simple MME. Detailed information is given in Jeong et al. (2012). Nino3 SST index (5°S – 5°N , 150°W – 90°W) and El Niño Modoki index are used to represent the two types of ENSO. The El Niño Modoki index is defined as the difference of SST anomaly in the central Pacific (10°S – 10°N , 165°E – 140°W) and the mean of SST anomaly at (15°S – 5°N , 110°W – 70°W) and (10°S – 20°N , 125°E – 145°E) (Ashok et al. 2007). The MME predictions show almost the same skill between the two types of ENSO at 1 month lead (0.94 vs. 0.91, Fig. 2.2). At 4 months lead, prediction skill of the Modoki index drops quickly while that of canonical ENSO remains unchanged (0.8 vs. 0.91).

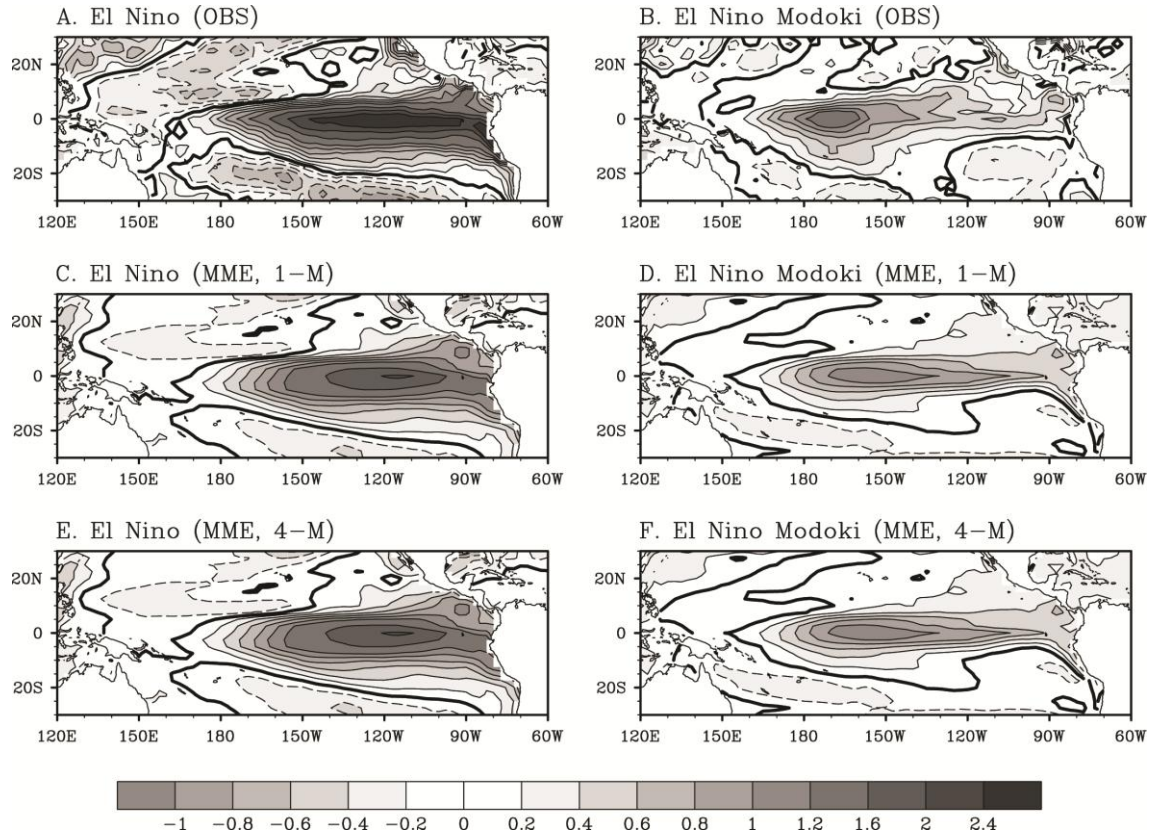


Figure 2.3: Composite SST anomalies of El Niño events (1982–1983, 1987–1988 and 1997–1998) and El Niño Modoki events (1994–1995, 2002–2003 and 2004–2005) during Dec-Jan-Feb based on observation (upper panels), 1-month lead MME predictions (middle panels) and 4-month lead MME predictions (lower panels). The left panels are for El Niño and the right ones are for El Niño Modoki (courtesy of Jeong et al. 2012).

Many current state-of-the-art OAGCMs have a difficulty in reproducing the distinct spatial distributions of SST anomalies between the two types of ENSO. Results based on the BoM model suggested the different SST anomaly patterns can be predicted up to less than one season ahead (Hendon et al., 2009)^b. Hindcasts of past three canonical El Niños (1982/83, 1987/88, and 1997/98) and three Modoki events (1994/95, 2002/03, and 2004/05) based on the multi-model predictions

show that the two distinct SST anomaly distributions during boreal winter can be well predicted up to at least 4 months ahead (Fig. 2.3). This suggests that memory for the evolution of the two types of El Niños should reside in the differences of ICs. The distinct impacts on global climate of the different types of El Niños are also predictable at short lead times (Jeong et al. 2012).

^bPrediction skill of the Modoki index is comparable to that of Niño3 index up to 6 months lead.

2.3. JAMSTEC SINTEX-F model prediction of ENSO up to 2-year lead

The JAMSTEC climate prediction system was built on the basis of the SINTEX-F fully coupled global OAGCM (Luo et al. 2003 and 2005a; Masson et al. 2005). The atmospheric component (ECHAM4.6) of the SINTEX-F model has a resolution of 1.1° (T106) with 19 vertical levels. Its oceanic component (OPA8) has a relatively coarse resolution of a 2° Mercator horizontal mesh but with an equatorial intensification up to 0.5° in meridional direction. It has 31 levels in vertical of which 20 lie in the top 500-m with a resolution of 10-m from sea surface to 110-m depth. Heat, water and momentum fluxes across the air-sea interface are exchanged every two hours without any corrections using a standardized coupler of OASIS2. No sea ice model is incorporated into the current system; sea ice cover is relaxed toward observed monthly climatology in the ocean GCM. The SINTEX-F model realistically simulates the ENSO and IOD variability, including their magnitudes, periods, and spatial patterns of SST anomalies (Yamagata et al. 2004; Luo et al. 2005a).

To generate realistic ICs for coupled model forecasts by developing complex schemes to assimilate available ocean and atmosphere observations is an important work, but requires extensive computing and human resources. Instead, a simple but effective initialization approach is adopted as an attempt to produce realistic and well-balanced ocean-atmosphere ICs by assimilating only observed SSTs in a coupled way (e.g., Luo et al. 2005b). After 11-year spin-up, model SSTs since 1 January 1982 are strongly nudged toward daily observations, which are

interpolated from weekly NCEP Reynolds analysis

(www.esrl.noaa.gov/psd/data/gridded/data.noaa.oisst.v2.html), by applying three large feedback values (-2400, -1200, and -800 W m⁻² K⁻¹) to the surface heat flux (Luo et al. 2005b, 2007, 2008a). They correspond to 1-, 2-, and 3-day restoring time for temperature in a 50-m surface mixed-layer, respectively. Interannual variations of the equatorial Pacific thermocline over the past 3 decades are well captured by using the coupled SST-nudging initialization scheme (see Luo et al. 2005b, 2010). Concerning large uncertainties in surface wind stress estimations, model coupling physics is further perturbed in three different ways by considering or neglecting ocean surface current contributions (Luo et al. 2005a). Therefore, the ensemble prediction system attempts to measure uncertainties of both ICs and model errors for forecasts. Based on this semi-multimodel ensemble prediction system, 9-member retrospective forecasts are performed for 24 target months from the first day of each month during February 1982 to December 2004. Since 2005, the JAMSTEC SINTEX-F prediction system has been used for real time forecast experiments with 27 members on a monthly basis and demonstrated excellent performance in forecasting ENSO and IOD and their related climate anomalies over the globe (see www.jamstec.go.jp/frsgc/research/d1/iod/e/seasonal/outlook.html).

All interannual ENSO events over the past three decades can be predicted by the SINTEX-F model up to 1-year lead (Fig. 2.4a, see also Luo et al. 2005b, 2008). Both the El Niño events in 1982/83, 1986/87, 1991/92, 1997/98, and 2002/03 and the La Niña events in 1984-86, 1988/89, 1995/96, 1999-2001,

2005/06, 2007-09, and 2010-12 are predicted up to 12 months ahead. During the period 1982–2012, there are only two small false alarms: a weak warm event in 1990/91 and a weak cold one in 2003/04. Predictions of the El Niños in the 2000’s appear to be less skilful compared to those in previous decades, a fact also found based on multi-model real time forecasts (Barnston et al. 2012; Wang et al. 2010). This is consistent with the change of El Niño characteristics in the 2000’s: while in previous decades equatorial warm SST ($>28^{\circ}\text{C}$), positive rainfall and warm subsurface temperature anomalies display an apparent eastward propagation in a coupled way in association with strong westerly anomalies in the central Pacific, the El Niño related warming and rainfall anomalies in the last decade tend to always stay in the western-central Pacific together with much weaker westerly anomalies in the central Pacific (Luo et al. 2012). There is also weak lead-lag relation between the equatorial warm water volumes and ENSO events in the last decade (Horii et al. 2012). We note that decadal cooling trends during the period 1991–1999 and 2002-2010 are well predicted up to two years ahead (see also Luo et al. 2008b). This suggests a potential predictability of the tropical Pacific decadal variations.

It is known that ENSO predictability decreases rapidly during boreal spring associated with the phase locking of ENSO with seasonal cycle; useful long-range forecasts must overcome this intrinsic prediction barrier. The SINTEX-F model can successfully predict ENSO across the first boreal spring barrier with correlations above ~ 0.5 but fails during the second one (Fig. 2.4b). In particular, predictions starting from 1 April and 1 May show ACC skills as high as

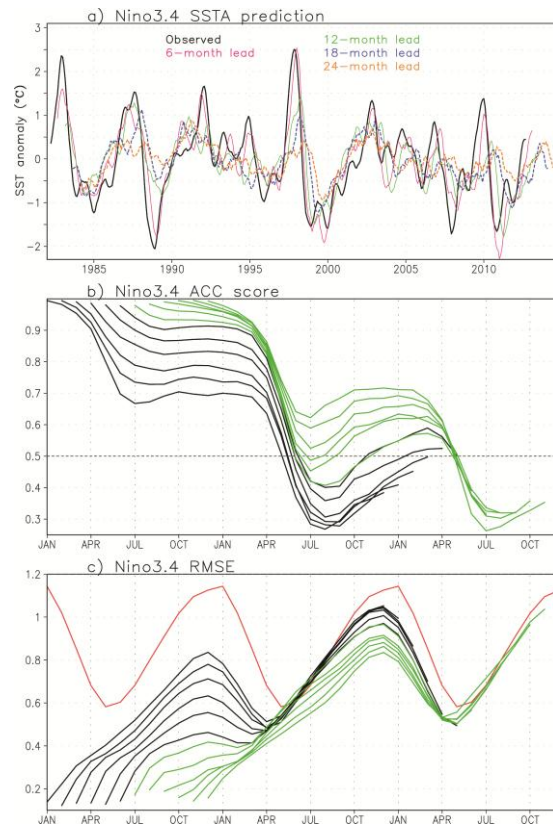


Figure 2.4: Prediction of the Niño3.4 SST anomalies. (a) The black curve is the observed (www.esrl.noaa.gov/psd/data/gridded/data.noaa.oisst.v2.html) and colour curves are 9-member ensemble mean retrospective forecasts at 6, 12, 18, and 24 months lead. Results have been smoothed with 5-month running mean. (b) Niño3.4 SST anomaly correlations between the observations and 9-member ensemble mean predictions up to 24 months lead. These are shown as a function of start month and lead time. (c) As in (b), but for the root mean square errors. The red line denotes one standard deviation of observed Niño3.4 SST index.

0.8 even at 1-year lead. It is encouraging that the prediction skill rebounds after crossing the first spring barrier and peaks in next boreal winter, coinciding with the evolution of ENSO. This is related to the correct prediction of subsurface signals in the equatorial Pacific (Luo et al. 2005b) which provide key memory for the development of the following ENSO

event. On average, ENSO prediction skill for the period 1982–2012 reaches about 0.6 (0.4) at 14 (24) months lead (Fig. 2.7) with root mean square errors smaller than 0.8°C. The ACC skill of 1982–2012 is about 0.1 lower than that of 1982–2004 (see Luo et al. 2008b). With increasing lead time, the RMSEs generally grow associated with decreasing ACC scores except for January–April: during this season the RMSEs diminish even though the ACC scores decrease (Fig. 2.4c). The RMSEs at mid-long lead times appear to follow the seasonality of ENSO variance. The RMSEs always tend to grow from May and reach maxima in November–January just before ENSO magnitude peaks and the RMSEs then decrease until next April. The results suggest that the prediction of ENSO onset (particularly El Niño onset) is more challenging than the prediction of ENSO decay. The forecast errors during June–November marginally exceed one standard deviation of Niño3.4 SST index, partly owing to the phase delay in the ENSO onset prediction.

It is encouraging that several ENSO events over the past three decades can be predicted even at lead times of up to 1.5–2 years (Fig. 2.4a, Luo et al. 2008b). Prediction of the strongest 1997/98 El Niño was found to be difficult and failed by most previous coupled GCMs beyond 6 months lead (e.g., Barnston et al. 1999). The SINTEX-F model is capable predicting this unprecedented event up to about 1.5-year lead with the forecasted amplitude reaching the 0.5°C criterion for El Niño definition. The predicted magnitudes at long-lead times (≥ 12 months), however, are much weaker than the observations and with a large phase delay in predicting the onset of this strongest El Niño event. This is partly due

to the large influence of massive westerly wind bursts in the western equatorial Pacific during late 1996 to mid-1997. The long-lasting La Niña events in 1984–86, 1999–2001, 2007–09, and 2010–12 are predicted well up to 1.5–2 years lead. The first two long-lasting La Niñas follow strong El Niños in 1982/83 and 1997/98 and the discharge process (Jin 1997) during the El Niños provides a good memory for the development of the two La Niñas (Luo et al. 2008b). However, no strong discharge signal is seen prior to the La Niñas in 2007–09 and 2010–12. Precise causes of the long-lead predictability of the two latest long-lasting La Niñas are yet to be understood. Amazingly, the intermediate El Niño event in 2002/03 is also predicted well up to 2-year lead; this suggests a link between the central Pacific El Niño (Modoki) and the tropical Pacific decadal variability. Seasonal climate anomalies over many regions of the globe during those ENSO years are also realistically predicted up to 2-year lead (Luo et al. 2008b, see also www.jamstec.go.jp/frsgc/research/d1/iod/e/seasonal/outlook.html).

Coupled OAGCMs have difficulties in producing and predicting the meridional width of ENSO SST anomalies and its teleconnections in the extratropics. Figure 2.5 shows the spatial patterns of both observed and predicted ENSO SST anomalies during its peak phase (Dec–Jan–Feb). ENSO magnitudes and the meridional broadness in the tropical Pacific are realistically predicted at lead times of up to 9 months and beyond. The cold SST anomalies in the central North and South Pacific, the warm anomalies along the eastern boundary in the North Pacific, the basin-wide warm signals in the tropical IO and the cold anomalies near the west coast of Australia are

well predicted. SST anomalies in the Atlantic are also reasonably predicted including the warm signal in the tropical North Atlantic and southeastern Atlantic and the cold signal in the equatorial Atlantic. During El Niño years, surface air temperature in boreal winter is generally warmer than normal over large parts of South America, Europe, Asia, and Africa as well as the western and eastern Australia (Fig. 2.5a). Cold (warm) winter conditions are found in the southeastern (northern) North America in association with the Pacific–North American (PNA) teleconnection pattern driven by ENSO. These are predicted reasonably well up to 9 months lead (Figs. 2.5b-d). The cold anomalies in the northern Eurasia (which has a weak link with ENSO) are realistically predicted at 3-month lead but not at 6-9 months lead.

Figure 2.6 shows the observed and predicted global precipitation anomalies during the peak phase of ENSO at 3, 6, and 9 months lead. Associated with El Niño events, generally more rainfall appears in the central and eastern equatorial Pacific, and less rainfall occurs in the Intertropical Convergence Zone and the South Pacific Convergence Zone (Fig. 2.6a). In the tropical IO, less (more) rainfall is observed in the eastern (western) region. These are successfully predicted at 3, 6, and 9 months lead (Figs. 2.6b–d). Besides, the drought in the northeastern Brazil, large parts of Australia, and South Africa and the floods near the west coast of the North America and east coast of the southeastern North America associated with the PNA teleconnection are also well predicted. Over the Indonesia region, however, the model shows a systematic wet bias in the rainfall predictions at all lead times. The wet bias is often seen in other models. Whether this could be caused by an insufficient resolution or deficiencies in model

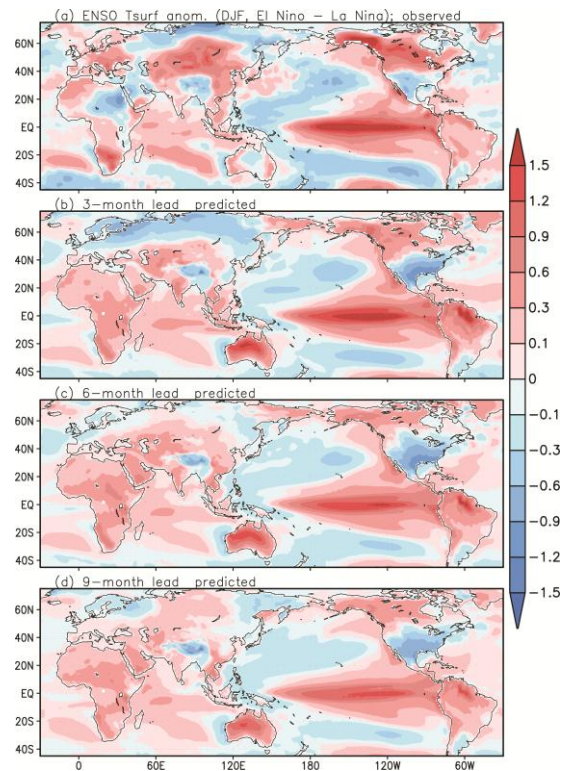


Figure 2.5: Differences of SST and terrestrial 2-m air temperature anomalies in boreal winter (Dec-Jan-Feb) between the 1982/83, 1986/87, 1991/92, 1994/95, 1997/98, 2002/03, 2006/07, and 2009/10 El Niño events and the 1984/85, 1988/89, 1995/96, 1998/99, 1999/2000, 2005/06, 2007/08, and 2010/11 La Niña events based on (a) the observations and (b-d) 9-member mean model predictions at 3, 6, and 9 months lead. Results have been divided by 2 in order to show the typical ENSO magnitudes. Observed 2-m air temperature is provided by NCEP reanalysis (www.esrl.noaa.gov/psd/data/reanalysis/reanalysis.shtml).

physics requires a further study. With increasing lead time, positive rainfall anomalies in the eastern equatorial Pacific gradually decrease in association with the development of a cold bias in the cold tongue area. This is another common bias to be addressed. We note that global precipitation anomalies of Jun-Jul-Aug in previous and following year (corresponding to ENSO onset

and demise season) are also predicted reasonably well up to 9-month ahead (Luo et al. 2005b).

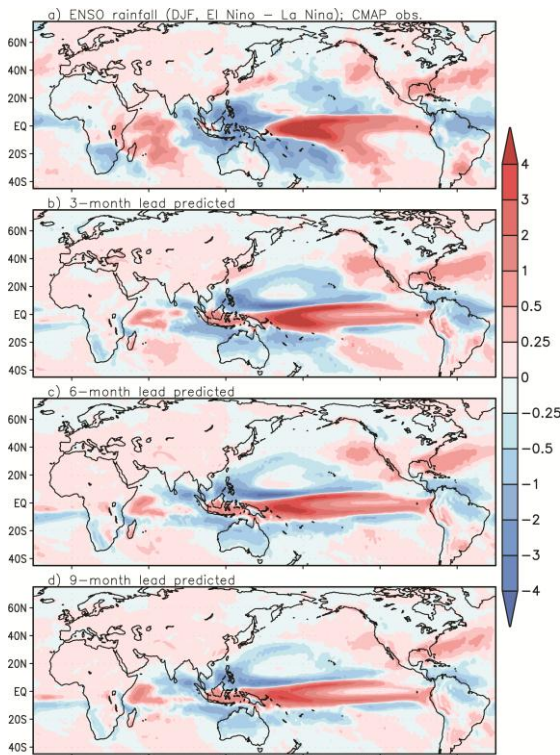


Figure 2.6: As in Fig. 2.5, but for the precipitation anomalies (unit: mm/day). Observed precipitation is provided by CMAP (www.cpc.ncep.noaa.gov/products/global_precip/html/wpage.cmap.html).

The SINTEX-F model predictions show that predictive skill of ENSO Modoki is fairly comparable to that of canonical ENSO at lead times of up to 2 years (Fig. 2.7). This is in contrast to the APCC multi-model prediction results presented in previous section. The skill difference between the Nino3 and Modoki indices is rather modest and not statistically significant. For the two indices, the SINTEX-F model prediction shows high skill (>0.6) up to about 12 months lead and medium skill of about 0.3 up to 2 years lead. The model

prediction skill of the two types of ENSO is well above the persistence prediction at all lead times (c.f., the solid and dashed lines in Fig. 2.7). Compared to the Nino3 index, the Modoki index shows high persistence, primarily owing to its dominant variance at decadal time scales. However, its high persistence does not give rise to higher prediction skill than the Nino3 index which shows dominant variance at interannual time scales. Interestingly, the Nino3.4 index—a mixture of the canonical and Modoki-type ENSO—has higher prediction skill than the two different ENSO indices at both short and long lead times despite of its relatively low persistence (black lines in Fig. 2.7).

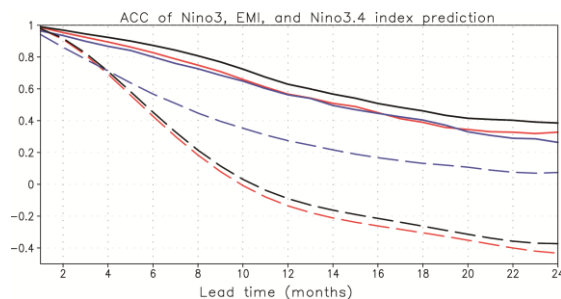


Figure 2.7: ACC skill scores (as a function of lead time) of Nino3 SST anomaly (red lines), ENSO Modoki index (blue lines), and Nino3.4 SST anomaly (black lines) based on persistence (dashed lines) and 9-member mean prediction of the SINTEX-F model for the period 1982–2012.

3. The IO climate and IOD prediction

Year-to-year climate variability in the tropical IO is largely driven by local ocean-atmosphere interactions and remote influence of ENSO. The IOD is an ENSO-like air-sea coupled climate phenomenon in the warm tropical IO (e.g., Saji et al. 1999). IOD usually starts in

boreal summer, peaks in fall, and decays rapidly in early winter, subject to the seasonal modulation by the East Asian-Australian monsoonal winds. The IOD can be driven by ENSO or sometimes independently arise from the local air-sea coupling (e.g., Luo et al., 2008b, 2010). Positive IOD features strong anomalous SST cooling in the eastern Indian Ocean (EIO) and weak warming in the west during boreal summer and fall, and vice versa for negative IOD. Without ENSO's influence, the intrinsic period of IOD is about 2 years, mainly controlled by a delayed negative feedback transmitted in the subsurface IO (Behera et al. 2006). Owing to active convection over the warm waters in the IO, IOD often causes profound environmental and socioeconomic impacts on not only the countries surrounding the IO but also various parts of the world. For instance, the 2006 IOD event caused large societal and economical losses, including the severe haze problem in Indonesia due to forest fires, exceptionally long lasting drought in Australia, and many deaths in East Africa due to floods. This suggests the importance and societal benefits of IOD prediction.

While ENSO-forced signals in the IO show high predictability, IOD itself has limited predictability (e.g., Wajsowicz 2005; Luo et al. 2005 and 2007; Wang et al. 2009; Shi et al. 2012). This is because: 1) air-sea coupling related to IOD is usually weak and more localized compared to ENSO; 2) the IO climate is affected by more complicated physical processes such as the strong Asian monsoon, and chaotic intraseasonal oscillations in both the atmosphere and ocean; 3) current state-of-the-art coupled OAGCMs for IOD forecasts still suffer from large deficiencies in simulating the IO climate; 4) large errors exist in the ICs owing to sparse

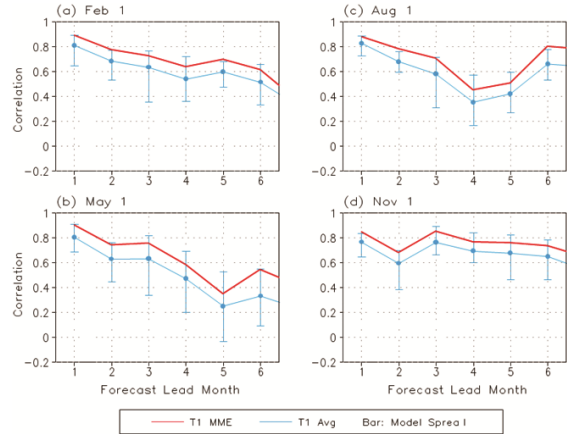


Figure 3.1: ACC skill for West Indian Ocean (WIO, 10°S-10°N, 50°-70°E) as a function of forecast lead time, initiated from (a) February 1, (b) May 1, (c) August 1, and (d) November 1 for the period of 1981-2001 derived from 14 coupled models that participated in CliPAS and DEMETER projects. The mid-blue lines indicate the averaged skill of the individual models and the bars show the range of the best and worst coupled model skills. The red lines denote the 14 coupled models' MME mean prediction skill.

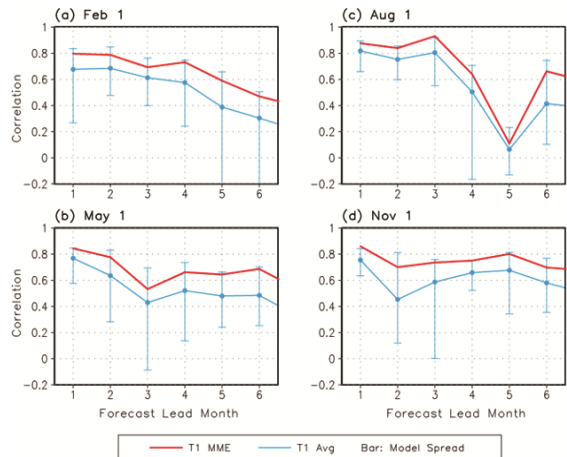


Fig. 3.2: As in Fig. 3.1, but for the East Indian Ocean (EIO, 10°S-0°, 90°-110°E) SSTA.

observations in the IO. Existing studies have suggested that IOD can be mostly predicted up to 1-2 seasons ahead although some extreme positive IOD events are predictable at long-

lead times of up to 1 year. We note that a large asymmetry exists between the surface warming and cooling intensity in the EIO associated with negative and positive IOD events (Hong et al. 2008). Negative IOD events do not appear to evolve into strong air-sea coupled processes in the IO, and therefore their peak magnitudes are weak with low predictability in general (Luo et al. 2007).

3.1. a. Multi-model prediction of IOD up to 6 months lead

Predictive skill of the IOD and individual poles up to 6 months lead were assessed based on the 13 coupled models (recall Table 2) that participated in CliPAS and DEMETER project. Figure 3.1 showed that the MME's ACC skill for the western IO (WIO) SST anomaly reaches 0.8 and 0.7 at 6-month lead for the predictions initiated from August 1 and November 1, respectively, although there is a considerable dip in skill in November for the forecast initiated from early August and a dip in December for the forecast initiated from early November. The EIO SST anomaly is more predictable with November and May initial condition than February and August initial condition (Fig. 3.2). There is a considerable forecast dip in December for the forecast initiated from early August. On average, the MME's ACC skill reaches 0.6 at 6-month lead.

While the SST predictions in the WIO and EIO show some useful skills, skill of the IOD index (i.e. SST anomaly gradient between the WIO and EIO) is reduced (Fig. 3.3). The forecast skill drops below 0.4 at 3-month lead for February and May initial condition and at 6-month lead for August and November initial condition. As Wang et al. (2009) indicated,

there are a July prediction barrier and a severe unrecoverable January prediction barrier for the IOD index prediction. Luo et al. (2007) showed that the unique winter barrier for prediction of IOD and the EIO SST is related to its strong phase lock to the annual reversal of the monsoon. For the forecasts started from early May, while a July barrier exists, there is a robust bounce-back after July; this suggests that the mature phase of IOD in October-November is more predictable probably due to the predictability of the EIO pole where the SST dominates the mature phase of IOD.

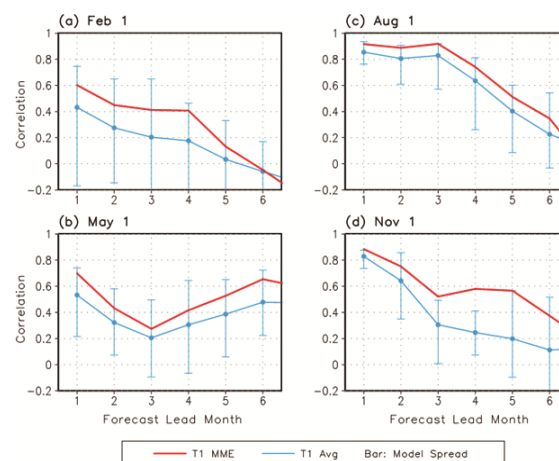


Fig. 3.3: As in Fig. 3.2, but for the Indian Ocean Dipole (IOD) SSTA index, which is the difference between WIO and EIO SST anomaly.

3.2. JAMSTEC SINTEX-F model prediction up to 1-2 years lead

It was found that SST anomaly in the EIO dominates the variability of IOD, while SST anomaly in the WIO is more controlled by ENSO. Unstable growth of strong surface cooling in the EIO is closely related to the Bjerknes feedback between strong coastal upwelling, SST gradient and surface winds

(Meyers et al. 2007, Luo et al. 2007, 2010); this plays a key role in initiating the IOD evolution. For simplicity, the EIO SST index is adopted to assess the predictive skill associated with IODc. Fig. 3.4 shows its skill based on 9-member ensemble mean prediction at lead times of up to 24 months. The results show a rapid drop of skill with increasing lead time starting from every month; the skill reaches minima around December (Fig. 3.4a), which is consistent with the rapid demise of IOD signal during boreal winter. This is distinct from the well-known spring barrier of ENSO. The IOD skill rebounds in late boreal winter/early spring and then declines again in late spring; this spring prediction barrier is related to ENSO's influence (Luo et al. 2005b). On average, the EIO SST index is predictable (with ACC >0.5) at lead times of up to about 2 seasons although some extreme positive IOD events are highly predictable even at 1-year lead (Luo et al. 2007, 2008b, 2010). It is interesting that skill of the EIO SST anomaly rebounds again in boreal fall of the next year and reaches a maximum in winter season but declines again in following spring. The long-lead predictability is coherent with that of Nino3.4 SST index (recall Fig. 2.4b); this suggests that such a long-lead predictability of IOD may arise from ENSO's influence. The variance of the EIO SST index shows an apparent annual cycle with a maximum in

boreal fall, consistent with the peak phase of IOD, and a minimum in boreal winter, consistent with the demise phase of IOD (Fig. 3.4b). The model forecast errors are generally less than or close to one standard deviation of the observation at lead times of up to about 2 years except those during boreal summer-fall at long lead times (associated with minimum ACC skills). The results suggest that, in general, IOD is hardly predicted at lead times beyond about 1 year.

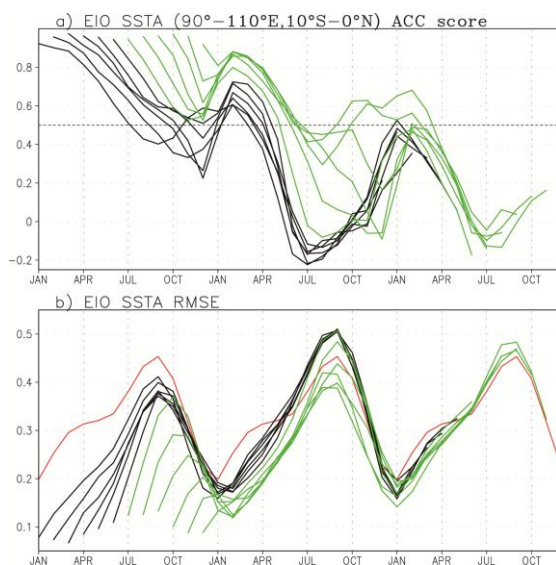


Figure 3.4: ACC of the EIO SST anomaly between the observations and 9-member ensemble mean predictions up to 24 months lead for the period 1982–2012 based on the SINTEX-F model. These are shown as a function of start month and lead time. (b) As in (a), but for the root mean square errors. The red line denotes one standard deviation of observed EIO SST index.

^c Skill of the IOD index is often lower than that of individual poles (Luo et al. 2007; Wang et al. 2009). This is not surprising since predicting the gradient of anomalies is usually more difficult than predicting the anomalies themselves. Correct prediction of the IOD index requires correct prediction of both the eastern and western poles. We note that, however, exceptional case occurs in the NCEP forecast system in which error cancellation between the eastern and western pole predictions leads to a better skill of IOD index compared to the individual poles (Shi et al. 2012).

Figure 3.5 shows the observed and predicted surface air temperature and precipitation anomalies around the IO during the peak phase of IOD (i.e., Sep–Nov) associated with the three extreme positive IOD events in 1994, 1997, and 2006. While the 1997 IOD co-occurred with a strong El Niño, the other two IODs co-occurred with weak-to-

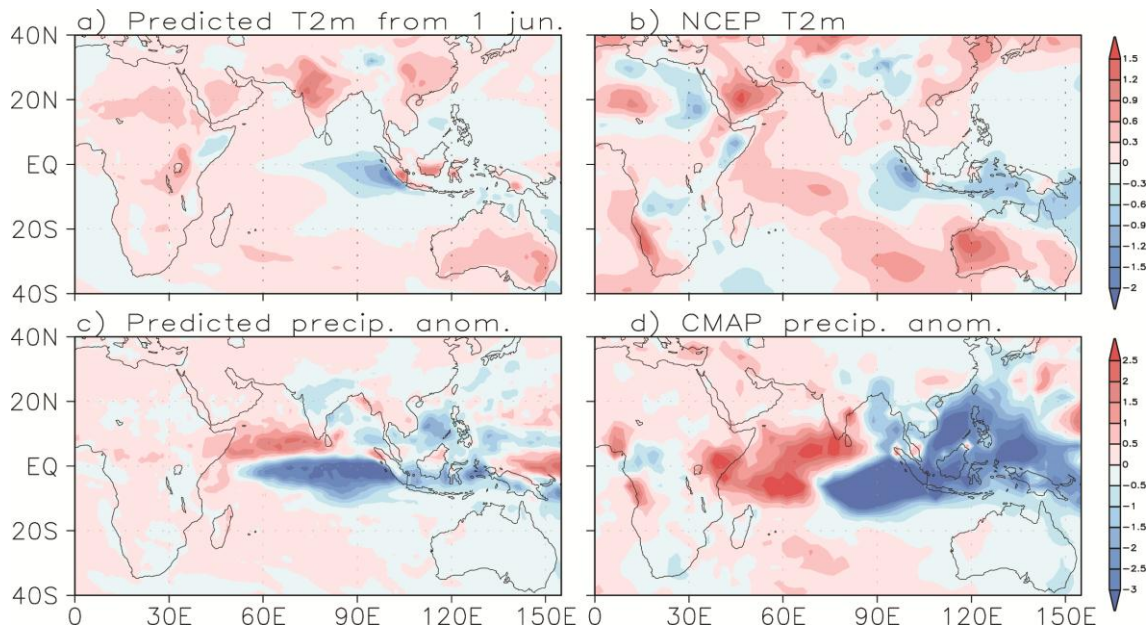


Figure 3.5: Composite maps of 2-m surface air temperature and precipitation anomalies in boreal fall (Sep-Oct-Nov) associated with three extreme positive IOD events in 1994, 1997, and 2006. These are based on observations (right panels) and the SINTEX-F 9-member ensemble mean predictions initiated from 1 June (left panels).

intermediate El Niños (or Modoki events). The model predictions are initiated from 1 June when the IOD usually starts to grow. Associated with the extreme positive IOD, strong cold SST anomalies ($<-1^{\circ}\text{C}$) appeared along the west coast of Sumatra with weak warm anomalies in the western IO. The extreme IOD induces large rainfall deficit in the EIO, Indonesia and the Philippines, and floods in WIO, South India, and East Africa. Besides, its remote influence via the atmospheric bridge caused warm and dry anomalies over large parts of Australia, warm conditions in East Asia and Arabian continent (right panels in Fig. 3.5; see also Luo et al. 2008b, 2007). The dipole structure of the surface temperature anomalies in the tropical IO during boreal fall and their impacts on the Eastern Hemisphere climate were predicted reasonably well at 1–2 seasons lead (left

panels in Fig. 3.5). Compared to the observations, however, the cold surface temperature anomaly and drought in the EIO extended far too west. This is related to a common model bias, namely, the equatorial thermocline is too flat associated with too weak westerly winds in the model's climatology (e.g., Luo et al. 2007). The drought in Indonesia and the Philippines, floods in East Africa and South India, and the dry and warm anomalies in Australia, warm conditions in East Asia and Arabian continent were predicted, albeit with some local discrepancies. The results suggest a potential predictability of not only the IOD signal itself but also its remote climate influences.

Except for the IOD which has its own predictability, climate variability in the tropical IO is largely controlled by ENSO. The SINTEX-F model shows that the highest skill

in the IO appears in the equatorial IO basin (IOB), southwestern IO (SWIO), and west of Australia (WA). Figure 3.6 shows the observed and model predicted SST anomalies in the three regions at 3, 6, 9, and 12 months lead. Interannual fluctuations in these regions are highly correlated with ENSO. Correlations among Nino3.4, IOB and SWIO indices reach above 0.6 when Nino3.4 leads 4 months. While the WA SST anomaly shows pronounced decadal variations, its correlation with Nino3.4 index reaches about -0.5 at 5 months lead. The model shows high skill in predicting the SST anomalies in the three regions. Almost all interannual anomalies in these regions associated with ENSO are well predicted up to 1 years lead despite some phase delays. The decadal fluctuations in the WA area are also well predicted. ACC skill reaches above 0.6 at the lead times of up to 10, 14, and 10 months based on the model 9-member ensemble mean predictions of the IOB, SWIO, and WA SST anomalies.

3.3. Interactions between the Pacific and IO

The Walker Circulation in the equatorial atmosphere, particularly the easterly (westerly) trade winds in the Pacific (IO) driven by the strong convection over the warm waters in the EIO-Maritime Continent-western Pacific, could be regulated by and play an important role in redistribution of the warm waters in the Indo-Pacific region, in association with ENSO and IOD evolution. For example, El Niño usually warms the IO basin, which in turn helps to increase the Pacific trade winds and hence in turn weaken El Niño. In particular years strong basin-wide warming in the IO may further trigger the phase transition from El Niño to La Niña (e.g., Kug et al. 2006). Recent studies also found interactions between

El Niño and IOD (Behera et al. 2006; Luo et al. 2010). For instance, the surface cooling in the EIO associated with the IOD may affect both concurrent and following El Niño (Luo et al. 2010; Izumo et al. 2010, 2014). The Indo-Pacific inter-basin coupling is crucial to the evolution of both El Niño and IOD and their predictability at long-lead times.^d After their onsets, however, contributions of the inter-basin coupling to their subsequent growth become limited owing to the dominant role of the local Bjerknes feedback in the individual ocean basins (Luo et al. 2010). The inter-basin coupling may also act on the Indo-Pacific centennial and multi-decadal changes (Luo et al. 2012). It was found that the fast SST warming in the IO over past 2-3 decades might have played an important role in modulating the Pacific Walker Circulation.

Improving the seasonal forecast of the IO climate variability can eventually lead to more skilful ENSO forecasts, and vice versa. The net gain in skill comes from the inter-basin coupling and independent sources for the predictability of ENSO and IOD. Based on the SINTEX-F model, influence of the inter-basin coupling on the predictions of tropical climate was examined by suppressing air-sea coupling in the tropical IO and Pacific, respectively. Monthly climatological SSTs of observations during 1983-2006 were prescribed in the individual ocean basins between 25°S and 25°N. By doing this over the basin without air-sea coupling, the atmosphere there will respond to the climatological observed SST, rather than predicted SST, during the 12-month forecast period. That is, oceanic feedbacks to the atmosphere there are

^d Note that interactions with the Atlantic are also important (e.g., Keenlyside et al. 2013). This issue, however, is beyond the scope of this article.

suppressed, and thereby the interacting feedbacks between the IO and Pacific via the atmospheric bridge (particularly the Walker circulation) are suppressed. The same model ICs used for the 9-member retrospective forecasts, generated by the coupled SST-nudging initialization approach, were used for the two sensitivity forecast experiments. Readers are referred to Luo et al. (2010) for more details of the sensitivity prediction experiments.

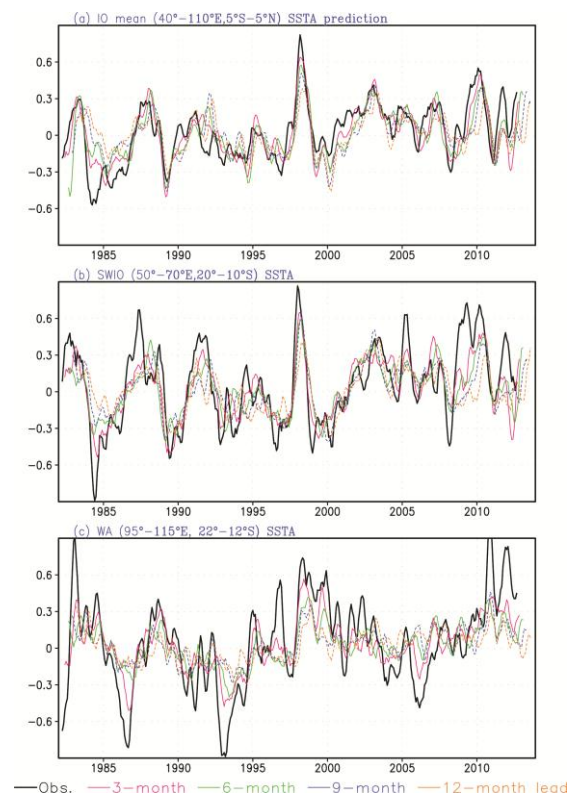


Figure 3.6: Predictions of SST anomalies in the equatorial Indian Ocean (5°S – 5°N , 40°E – 110°E ; IOB), southwestern Indian Ocean (20°S – 10°S , 50°E – 70°E ; SWIO), and west of Australia (22°S – 12°S , 95°E – 115°E ; WA). Black, red, green, blue, and yellow lines denote the observed, 3-, 6-, 9-, and 12-month lead predictions based on the SINTEX-F 9-member mean hindcasts. ACC skills reach >0.6 at the lead times of up to 10, 14, and 10 months for the SST anomalies in the three regions of the Indian Ocean.

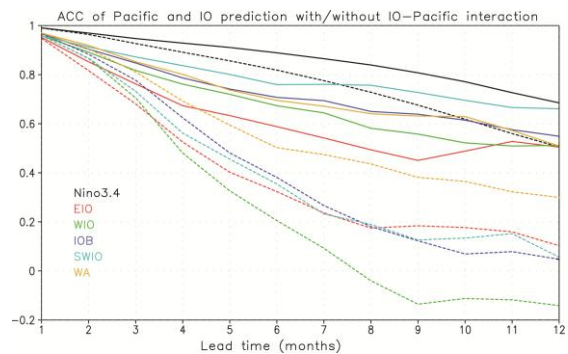


Figure 3.7: ACC skills of Nino3.4, EIO, WIO, IOB, SWIO, and WA SST anomalies based on the 9-member ensemble mean predictions with (solid lines) and without (dashed lines) the IO-Pacific inter-basin interactions. 12-month hindcasts are conducted every month during the period 1982–2006. Local air-sea coupling in the tropical Pacific and IO is removed separately to assess the influence of IO-Pacific inter-basin interactions on the climate prediction skills in the two basins.

Large influence of the IO signals on El Niño evolution is found during extreme IOD years (Luo et al. 2010). For instance, the Modoki-type El Niño in 1994/1995 was found to be fully driven by the strong 1994 IOD despite the Pacific subsurface cooling precondition in 1994. Owing to the large impact of ENSO on the IO, skill of the IO climate prediction would be much reduced if the ENSO signal were suppressed (colour lines in Fig. 3.7). This is particularly true for predictions of the SST anomalies in the WIO, IOB and SWIO near the Seychelles-Chagos dome. The skill reductions in the three regions reach as much as about 0.5–0.6 at 12-month lead. Without the ENSO influence, useful prediction skill ($\text{ACC} > 0.5$) of the SST anomalies in the three regions can be obtained up to only 4–5 months lead (in contrast to the useful skill up to >12 months lead in the presence of ENSO's influence). This clearly suggests that the local SST variations in the

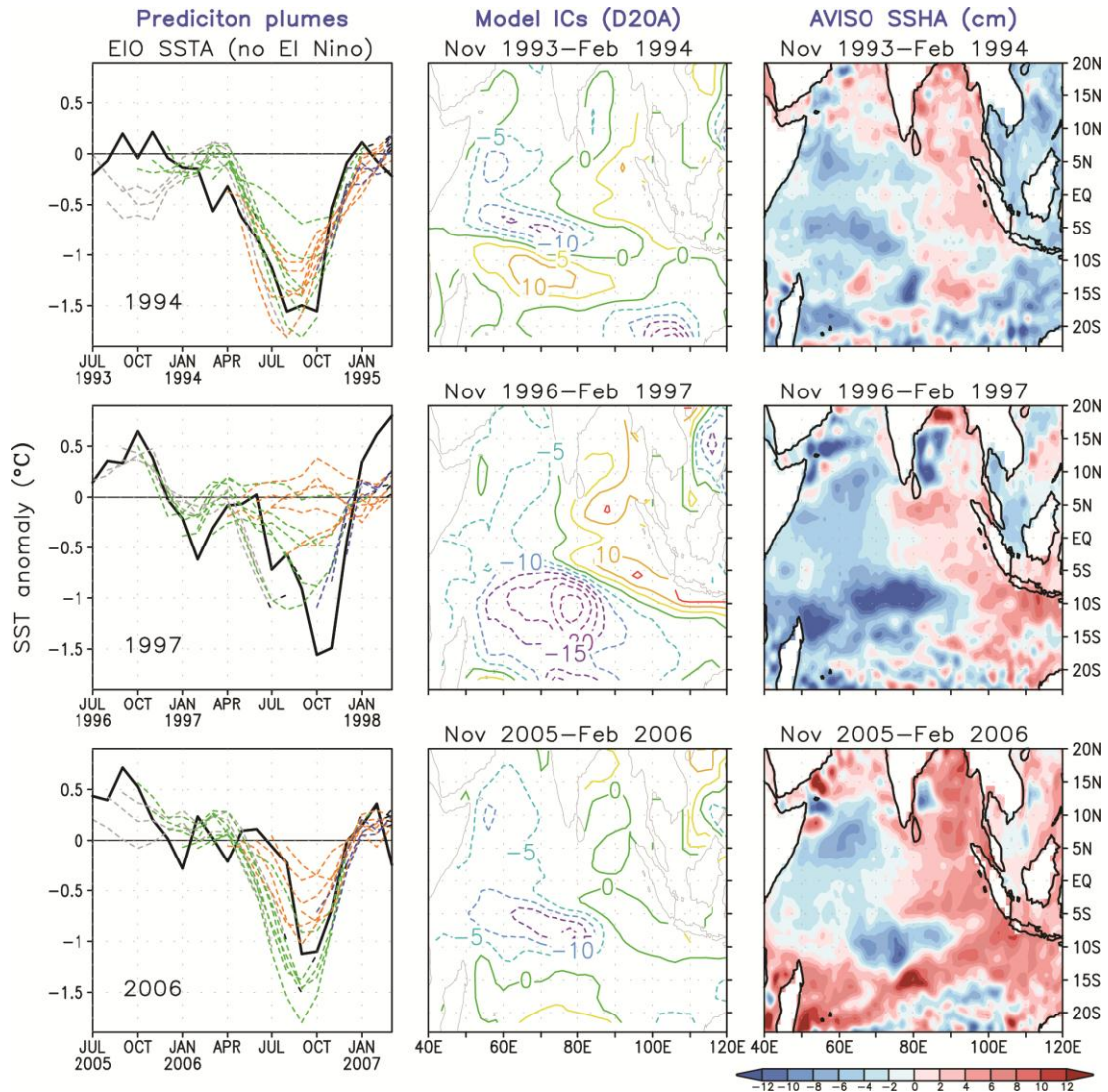


Figure 3.8: (left panels) The SINTEX-F predictions of the EIO (90°-110°E, 10°S-0°) SST anomalies associated with the three extreme positive IOD events in 1994, 1997, and 2006 after the Pacific El Niño signal is removed during the model 12-month forecasts. The black curves are observations and colour curves 9-member mean forecasts for 12 target months. Three gray lines indicate the forecasts initiated from 1 July, 1 August, and 1 September of the year before the IOD, six green lines are the predictions starting from the next 6 consecutive months, and so forth for the six orange and three blue lines. (middle panels) 20°C isotherm depth (D20, in meters) anomalies based on the model 9-member mean ICs from Nov to Feb prior to the occurrence of each extreme IOD. (right panels) As in (middle panels), but for the sea surface height anomalies (unit: cm) based on satellite observations. Courtesy of Luo et al. (2007, 2010).

three regions are predominantly controlled by ENSO. One exception, however, is found in the WA where certain predictability of the

SST anomaly at mid-long lead times appears to be maintained by its decadal variations (recall Fig. 3.6c).

In summary, the results indicate that ENSO's influence on the IO is much larger than the IO's influence on ENSO. Compared to the WIO, the EIO SST anomaly shows less prediction skill even in the presence of ENSO's influence at both short and long lead times (c.f. red and green lines in Fig. 3.7). This is because the EIO SST anomaly is partly driven by the local air-sea coupling, whereas the WIO SST anomaly is mostly controlled by ENSO. The local air-sea interactions in the IO, albeit weak compared to ENSO, produce independent predictability of IOD particularly during extreme positive IOD years (e.g., Luo et al. 2007, 2008b, 2010). Model results, based on sensitivity prediction experiment in which air-sea coupling in the tropical Pacific is suppressed (hence no El Niño influence), suggest that the three extreme IOD events in 1994, 1997, and 2006 can still be well predicted up to 1-year ahead (left panel in Fig. 3.8). The internal precursor for the long-range predictability of the extreme IOD in the model comes from the strong anomalous subsurface cooling in the SWIO; this is confirmed by satellite-observed sea level height anomalies (c.f. middle and right panels of Fig. 3.8). The cold subsurface anomaly in the SWIO in boreal winter prior to the development of IOD, that is a response to the cyclonic-like wind forcing in the east about one season ahead (Xie et al. 2002; Rao et al. 2002; Luo et al. 2010), propagates westward to the western boundary and then reflects as eastward-propagating equatorial upwelling Kelvin waves in the following seasons (Behera et al. 2006). This provides a long-lead precursor for the extreme IOD evolution (Horii et al. 2008; Luo et al. 2007, 2008b, 2010).

4. Prediction of subtropical dipole modes and southern African climate

Compared to the tropics, climate predictability in extratropics is generally low owing to large atmospheric internal variability and weak local ocean-atmosphere coupling, except areas where tropical climate has strong influences. Recent studies found two significant subtropical northeast-southwest-orientated dipole modes of SST anomaly in the South Atlantic and IO that may have impacts on the southern African climate (Venegas et al. 1997; Behera and Yamagata 2001; Morioka et al. 2010, 2011). The dipole SST anomalies are mainly forced by the atmospheric circulation anomalies, whereas the oceanic processes play negligible roles (Morioka et al. 2010; Kataoka et al. 2012). Hence, successful prediction of large-scale atmospheric circulation anomalies is essential for the prediction of the South Atlantic Subtropical Dipole (SASD) and IO Subtropical Dipole (IOSD) modes. The two dipole modes are well simulated and predicted by the SINTEX-F model (Morioka et al. 2012; Yuan et al. 2014a).

The prediction skill for the SASD and IOSD indices (defined as differences in SST anomalies between the southwestern and northeastern poles) and SST anomalies in individual poles are examined. ACC skill of the SASD index is 0.6, and normalized root mean square error (NRMSE) is 0.8 at 3-month lead (Figs. 4.1a-b). For all the 1-12 month lead predictions, the SINTEX-F model predicts the SASD better than the persistence with the skill of individual poles being comparable (Figs. 4.1c-f). Seasonally stratified ACCs of the SASD index (Fig. 4.2a) show that the prediction skills are high in austral summer no matter which month the prediction is

initialized from. This may be due to both the seasonal phase-locking behaviour of the SASD and the strong tropical influences in austral summer. The seasonal phase-locking behaviour in the two poles is well predicted (Figs. 4.2b-c). ACC skill of the IOSD index is over 0.7 up to 2-month lead, but drops below 0.6 at 3-month lead owing to the quick drop in the southwestern pole (Figs. 4.3a, c, e). While the seasonality of the northeastern pole is predicted, the model fails in the southwestern pole and thus in the IOSD index (Figs. 4.2d-f). The overall prediction skills of the southwestern pole are lower than the

persistence (Fig. 4.3e). As a whole, the prediction skills for the IOSD are lower than the SASD and only slightly better than the persistence up to 6-month lead (Fig. 4.3a).

During the period of 1982-2010, six (four) out of seven (ten) negative SASD (IOSD) co-occurred with positive IOD and/or El Niño and six (three) out of eight (seven) positive SASD (IOSD) co-occurred with negative IOD and/or La Niña. The correlation coefficient between September-October IOD and SASD (IOSD) indices is -0.24 (-0.23), significant at a 10% level, and that between November-December Niño3 and SASD (IOSD) indices is

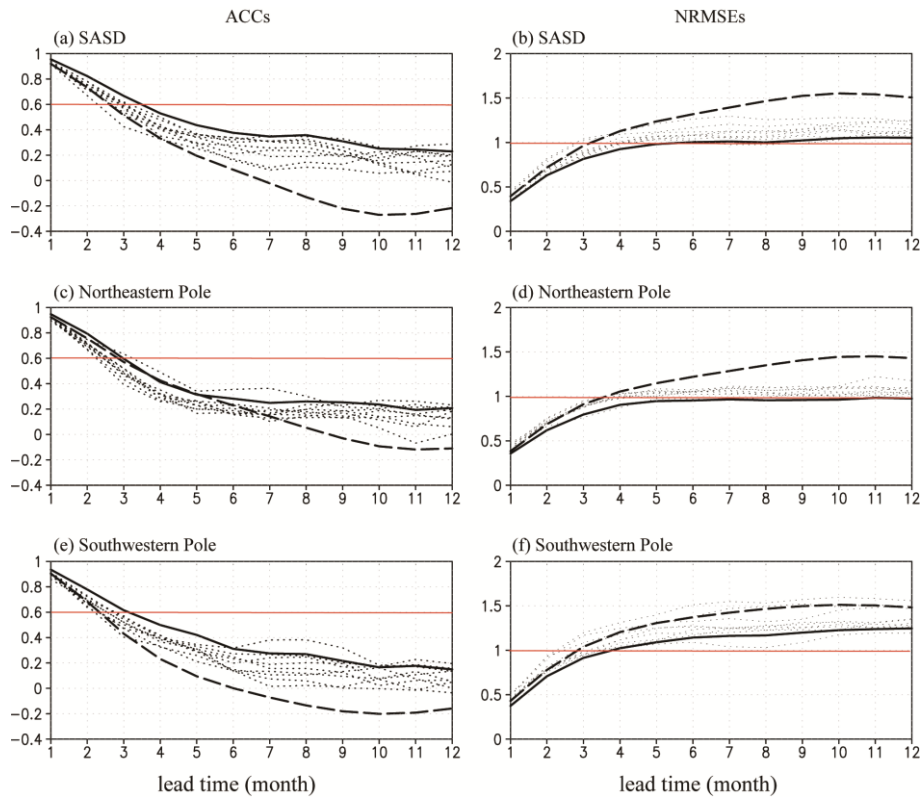


Figure 4.1: ACCs (left panels) and normalized root mean square errors (NRMSEs, right panels) of (a, b) SASD index and SST anomalies in (c, d) the northeastern and (e, f) southwestern poles. Black-dashed lines denote the persistence, black-solid lines the ensemble mean prediction, and black-dotted lines individual members. Red-solid lines denote 0.6 value of ACC (left panels) and 1.0 value of NRMSE (right panels). The standard deviations of the observed SASD index and SST anomalies in the northeastern and southwestern poles are 0.69 °C, 0.39 °C, and 0.42 °C, respectively. All the time series have been smoothed by a 3-month running mean before the skill calculation. Courtesy of Yuan et al. (2014a).

-0.59 (-0.27), significant at a 1% (10%) level. Linear combination of the sea level pressure (SLP) anomalies partially regressed on the IOD and ENSO indices from September-October to November-December shows a similar pattern to the observed that drives the 1997/98 negative SASD and IOSD (Yuan et al. 2014a). The results suggest that the IOD and ENSO may play a role in triggering the SASD and IOSD, and provide a source of predictability for the subtropical modes.

The southern Africa experiences distinct seasonality of precipitation with the wet season in austral summer and the dry season in

austral winter over most of its interior domain. Local agriculture is predominantly rain-fed and thus highly vulnerable to rainfall variations. It is found that the ENSO, SASD and IOSD often affect the southern African precipitation anomalies (e.g., Lindesay 1988; Behera and Yamagata 2001; Vigaud et al. 2009; Yuan et al. 2014b). Figure 4.4 shows the seasonally stratified ACCs and NRMSEs of the southern African precipitation index defined as the precipitation anomalies averaged over (11° - 41° E, 10° - 35° S). The ACC skill is larger than 0.4 for the austral summer precipitation anomalies and the NRMSE is

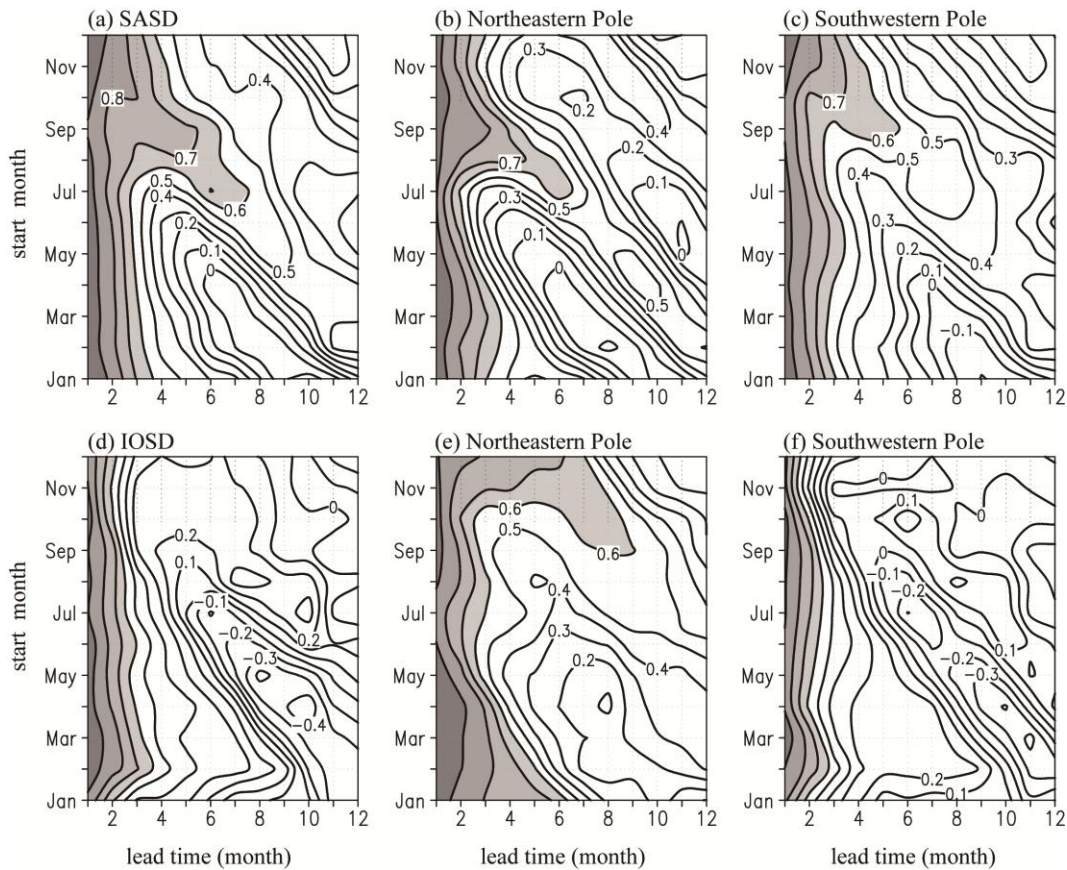


Figure 4.2: Seasonally stratified ACCs of (a, d) indices and SST anomalies in (b, e) the northeastern and (c, f) southwestern poles of (upper panels) the SASD and (lower panels) the IOSD as a function of start month and lead time. Areas with values of ≥ 0.6 are shaded. All the time series have been smoothed by the 3-month running mean before the calculation. Courtesy of Yuan et al. (2014a).

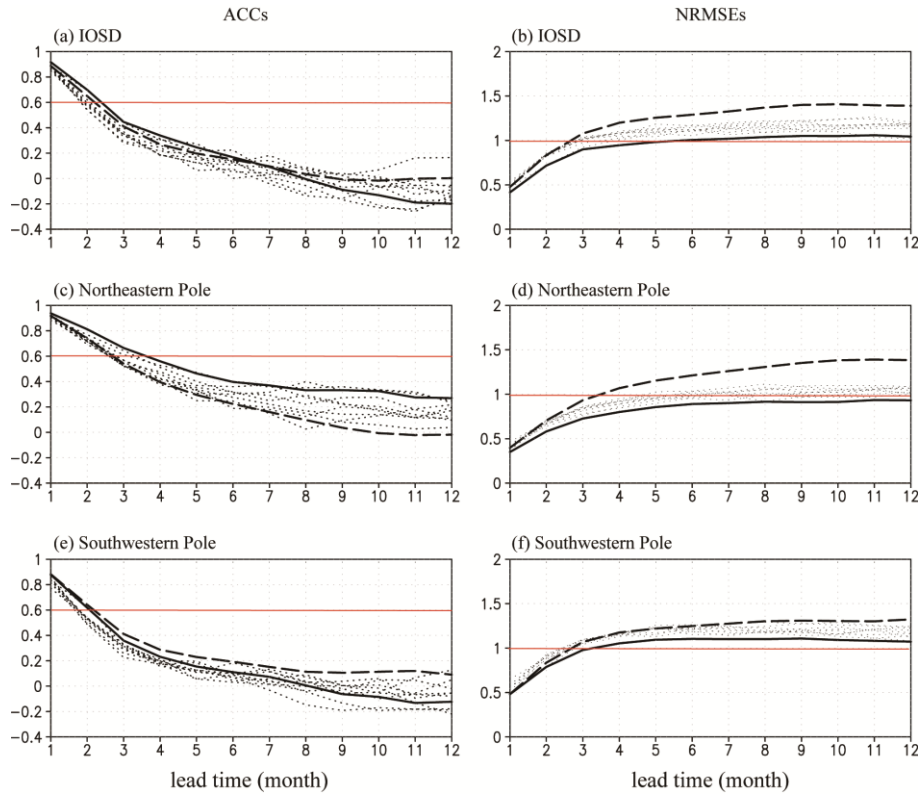


Figure 4.3: As in Fig. 4.1, but for the IOSD. The standard deviations of the observed IOSD index and SST anomalies in the northeastern and southwestern poles are 0.55 °C, 0.34 °C, and 0.38 °C, respectively. Courtesy of Yuan et al. (2014a)

around one standard deviation (0.29 mm day^{-1}). When the model is initialized from the 1st of October-December, the ACC of December-February precipitations is as high as 0.6. This good skill of the southern African summer rainfall prediction comes from the model's high skill in predicting ENSO and its related teleconnections over southern Africa (Luo et al. 2005b, 2008a; Yuan et al. 2014b).

Fig. 4.5 shows the SINTEX-F model's prediction skill for the surface temperature in southern Africa. The ACC is above 0.5 even

up to 12-month lead, much higher than the persistence except that at short lead times. Seasonally stratified ACCs show that the highest skills are mainly achieved in austral summer and autumn (December-May). The predictability in the two seasons mainly originates from the influences of ENSO. Spatial pattern of the model's skill is similar to that of observed correlation pattern between Nino3 index and the austral summer and autumn surface temperature. In addition to the atmospheric pathways, ENSO may influence the southern Africa climate via the IO SST variations. Warm (cold) SST anomalies in the

^e We use a broad area to define the land surface temperature index (i.e., the mean value over the continent south of the equator) since temperature variation is more spatially coherent than precipitation.

Using the same region as that of precipitation does not change our conclusions.

tropical and southern IO during El Niño (La Niña) induce the advection of warmer (colder) than normal airflows from the IO to southern Africa and result in the abnormally warmer (colder) surface temperature in southern Africa.

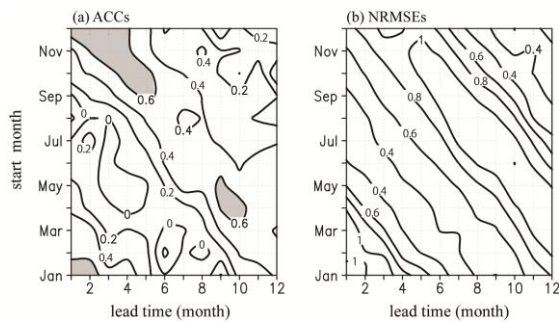


Figure 4.4: Seasonally stratified (a) ACCs and (b) NRMSEs of the southern African precipitations averaged over (11° - 41° E, 10° - 35° S) as a function of start month and lead time. Areas with values of ≥ 0.6 in (a) are shaded. One standard deviation of the observed (CMAP) southern African precipitation is 0.29 mm day^{-1} . Courtesy of Yuan et al. (2014a).

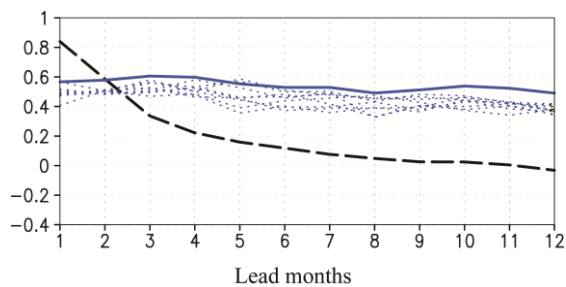


Figure 4.5: ACCs of 2-meter-height temperature (T2m) averaged over southern Africa south of the equator. Black-dashed line denotes the persistence, blue-solid line the ensemble mean prediction, and blue-dotted lines individual members.

5. Impact of global warming on seasonal prediction

Predictability of climate variations and climate changes has usually been treated separately. A

majority of studies on seasonal predictions including real-time experimental forecasts have neglected the potential influence of changing external radiative forcing, whereas much evidence shows that increasing GHG concentrations may have already exerted an important role in global warming, particularly over the recent decades (IPCC AR4 report, <http://www.ipcc.ch/>). Besides, the changing climate background can affect daily-to-interannual climate variations and the occurrence frequency of climate extreme events. Therefore, it becomes important and is of practical use to examine the role of historical GHG forcing in global climate predictability on seasonal-to-interannual time scales (e.g., Doblus-Reyes et al. 2006; Liniger et al. 2007; Luo et al. 2011). Recently developed climate prediction systems have now incorporated the impacts of time-varying anthropogenic and natural radiative forcings on short-term prediction. It is worth noting that current forecast systems with fixed (i.e., time-invariant) external radiative forcing are still able to predict global warming trend to some extent, particularly at short-mid lead times (Cai et al. 2009). This is because that the global warming signal is partly contained in the ICs of the climate system, especially the upper ocean. The SST rise plays a key role in driving the intensified terrestrial warming over the globe, and the long-memory of the upper ocean provides a limited predictability of global warming even with fixed GHGs emissions during the forecast (Luo et al. 2011).

Observed global mean (60° S- 75° N) 2-m surface air temperature anomaly has risen at a linear rate of $\sim 0.14^{\circ}\text{C}/\text{decade}$ during 1982-2012. To assess the influence of global warming on climate prediction: 1) we first calculate the ACC between non-detrended

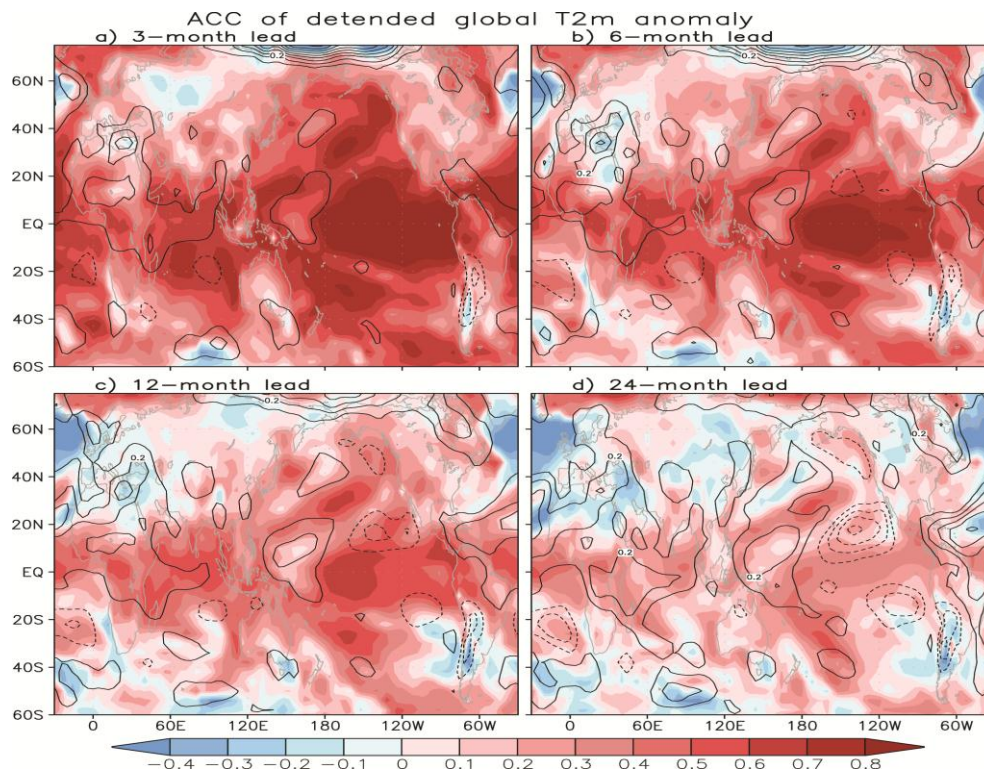


Figure 5.1: T2m anomaly correlations (colour scale) between the non-detrended observations and detrended model 9-member mean predictions at different lead times for the period 1982-2012. Shown also are the skill improvements (contour interval: ± 0.1 , ± 0.2 , ± 0.3 , ...) by assuming that the warming trend of the observed global mean T2m anomaly were perfectly predicted at all lead times (Luo et al. 2011). The skill is measured based on 4° by 4° grid cells.

observations and detrended model predictions by assuming that the model completely fails to predict the global mean warming trend; 2) potential skill due to global warming is estimated by assuming that the observed global mean warming trend is perfectly predicted at all lead times (see Luo et al. 2011). The skill difference between 2) and 1) provides a rough measure of the global warming impact on climate predictability. The global warming's impact varies from region to region (Fig. 5.1). Suppressing the predictability of the warming trend, the SINTEX-F model still shows good skill in predicting the surface air temperature anomalies over most parts of the globe (Fig.

5.1). Medium-to-high predictability is found over the oceans except the North Atlantic, whereas predictive skill of terrestrial surface air temperature anomalies is generally low-to-modest except in the tropics and some coastal areas. The highest predictability of the surface temperature anomalies at 1-2 years lead is mostly confined in the tropics (Figs. 5.1c-d) owing to strong tropical air-sea interactions there. Modest predictability at long-lead times is also found in some extratropical regions such as the North and South Pacific in association with ENSO teleconnections (Luo et al. 2008a, 2011).

Adding a perfect predictability of the global mean warming trend does not improve

much the predictability of the surface air temperature anomalies over most parts of the globe (except the Arctic Ocean) at 3-6 months lead (contours in Figs. 5.1a-b). Variance of the model predicted anomaly is often high and close to the observed at short lead times because the forecasts are initiated from as realistic as possible ICs. With the increasing lead times, growing ensemble spreads weaken the variance of ensemble mean forecast. Therefore, impact of the global warming on climate prediction generally increases with the increasing lead times. At long-lead (12-24 months) times (Figs. 5.1c-d), considerable improvements due to the global warming are found in the tropical IO-western Pacific and the tropical North Atlantic where the surface temperature shows warming trends in recent decades. In the tropical eastern Pacific where the surface temperatures have cooling trends, the predictability would be reduced by assuming a homogeneous warming trend over the globe. We note that the large skill difference in the Arctic Ocean at short-mid lead time may be caused by spurious ICs (hence negative skill) there where sea ice cover in the model is restored toward observed monthly climatology. Despite the negative skill at short-mid lead times, skill in the Arctic Ocean surprisingly increases and becomes significantly positive at long-lead times. This suggests that the Arctic Ocean surface temperature might be largely influenced by remote factors, possibly tropical climate.

Linear trends of the SST anomalies in the tropical Pacific during 1982-2012 display a La Niña-like pattern in association with an enhanced Walker cell (Luo et al. 2012). Owing to the compensation between the western warming and eastern cooling, warming rate of the tropical Pacific mean SST

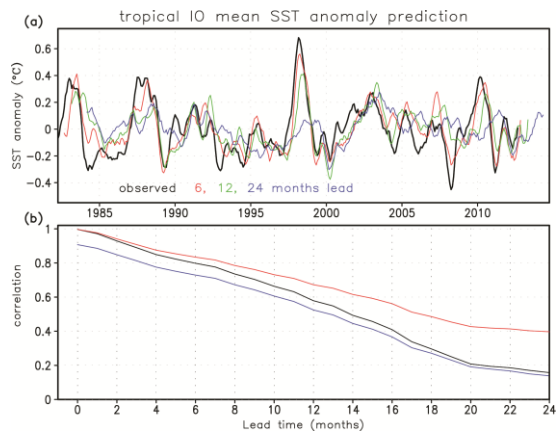


Figure 5.2: (a) Detrended tropical IO mean SST anomaly (40° - 120° E, 20° S- 20° N) based on the observations (black line), and the SINTEX-F model 9-member mean predictions at 6, 12, and 24 months lead (colour lines). (b) Model prediction skill of the tropical IO mean SST anomaly during 1982-2012 at lead times of 1-24 months. Black line denotes the predictability of natural variability (i.e., both the observed and predicted anomalies are detrended). Blue line indicates the correlation between non-detrended observations and detrended model prediction. Red line shows the predictability if the observed warming trend of the IO mean SST anomaly were perfectly predicted at all lead times.

(120° - 280° E, 20° S- 20° N) during 1982-2012 is nearly zero. In contrast, SSTs in the tropical IO has rapidly warmed up; warming rate of the IO mean SST anomaly (40° - 120° E, 20° S- 20° N) reaches $\sim 0.1^{\circ}$ C/decade. Natural variations (i.e., detrended) in the tropical IO are strongly determined by ENSO. Impacts of major ENSO events, such as the warming related to 1982-83, 1987-88, 1997-98, 2002-03, 2009-10 El Niños and the cooling related to 1984-86, 1988-89, 1999-2000, 2005-06, 2007-08, and 2010-11 La Niñas, are clearly seen (Fig. 5.2a). The interannual variations of the tropical IO mean SST anomaly are realistically predicted up to 13-14 months lead with ACC score of above 0.5 (Figs. 5.2 a-b).

At 24-month lead, the model basically predicts low-frequency components. The results are similar to the model’s ENSO predictions at lead times of up to 2 years (recall Fig. 2.4, Luo et al. 2008a). A perfect prediction of the IO mean warming trend would improve forecast skill of the SST anomaly at all lead times (c.f., blue and red lines in Fig. 5.2b). While the impact of the warming trend is negligible at short-mid lead times, the skill gain at long-lead times (>1 year) due to the warming trend becomes significant and is as large as the predictive skill of its natural variations at lead times beyond 20 months.

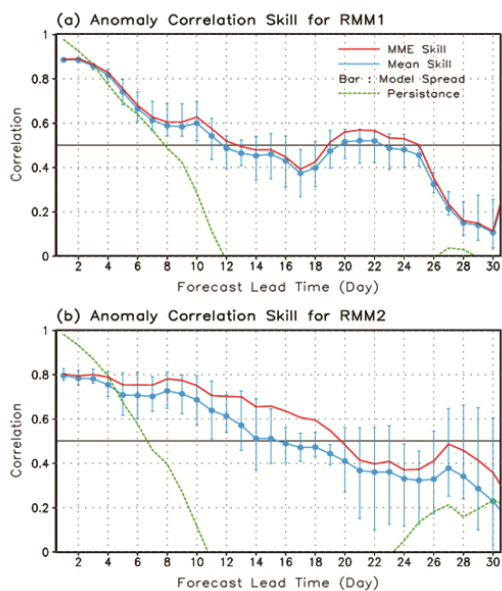


Fig. 6.1: The ACC skill for the (a) RMM1 and (b) RMM2 as a function of forecast lead time predicted by five coupled models and their MME mean initiated from 1 Nov for the 21 years of 1981-2001. For comparison, the persistence skill is also shown.

6. MJO prediction

The MJO is the dominant intraseasonal variability in the global climate system with quasi-oscillating period of 30-60 days

(Madden and Julian 1971) and significant impact on the local and remote aspects of weather and climate, including Asian, Australian and North American monsoons, tropical cyclones, and North Pacific atmospheric circulations (e.g., Lee et al. 2013; Hendon and Liebmann 1990; Lorenz and Hartmann 2006; Bessafi and Wheeler 2006; Moon et al. 2012). Achieving a better understanding of the MJO, its dynamics and predictability together with its associated weather and climate impacts are of importance for extending weather forecast beyond its current limit and developing seamless suite of weather and climate prediction. For the MJO, the 2-component Real-time Multivariate MJO (RMM) index (RMM1 and RMM2) developed by Wheeler and Hendon (2004) is the most widely used for monitoring and forecast applications. It is defined by the first two principal component time series of the multivariate empirical orthogonal function modes of the equatorial mean (between 15oS and 15oN) outgoing longwave radiation and zonal wind at 850 and 200hPa. The equatorial symmetric nature of the RMM index makes it an excellent measure of the equatorial eastward propagating MJO during Dec-Feb. With the improvement of OAGCMs’ performance in simulating MJO in recent decades (Sperber and Waliser 2008), predictive skill of MJO has been increased rapidly. While early predictions based on AGCMs achieved a useful skill up to only ~7 days ahead for Dec-Feb (e.g., Hendon et al. 1999), a majority of operational forecast models can now produce useful skill of >0.5 up to 15 days ahead (Zhang et al. 2013). It was suggested that the MJO skill can be further improved using a MME approach (Wang et al. 2009) although difficulty exists in collecting quality long-term multi-model hindcast data

sets. To evaluate the MME skill for the MJO prediction, here we first use five coupled models' hindcast that participated in DEMETER project (Palmer et al. 2004). All five models have daily hindcast initialized from 1 Nov for the 21 years of 1981-2001. Thus, the total forecast sample size is 21. Figure 6.1 shows the ACC skill for the RMM1 and RMM2 prediction initiated from 1 Nov for the 21 years using individual models and their simple MME with equal weight. It is noted that the MME has a useful skill of 0.5 up to 20-25 days lead for the RMM1 and RMM2 prediction. Although the MME's skill is not always better than the best model's skill, even the simple MME is generally better than individual models.

Motivated by significant societal demands for reliable subseasonal prediction, the coordinated Intraseasonal Variability Hindcast Experiment (ISVHE) was launched in 2009.

The project aims to determine intraseasonal predictability and realized prediction skill in the current dynamical models. The ISVHE project is the first attempt to produce a long-term hindcast dataset that specifically targets the needs and themes associated with intraseasonal prediction research. Currently, hindcast datasets produced by 12 models have been collected from six operational centers and six research groups (see <http://iprc.soest.hawaii.edu/users/jylee/clipas/>), covering the period from January 1989 to December 2008 initiated either every 10 days in each calendar month or every first day of each month for at least 45-day integrations.

Analysis of the 12 climate models' hindcast data in the ISVHE indicates significantly improved MJO forecast skill. The ACC skill for the RMM1 and RMM2 is assessed initiated from the first day of month

from November to April for the 20 years of 1989-2008. Thus, the total forecast sample size is 120. Figure 6.2 indicates that the MME with the most recent climate models has a useful skill for the MJO prediction up to 26-28 days ahead. On the other hand, MJO predictability estimated by ISVHE ensemble-mean hindcasts is on the order of 35-45 days (Mani et al. 2014).

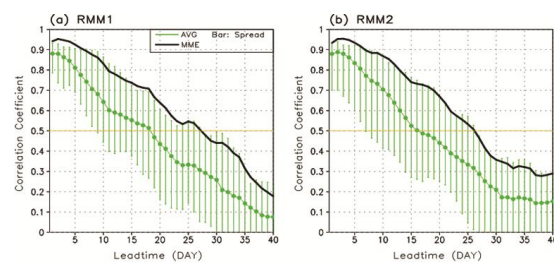


Fig. 6.2: Same as Fig. 6.1, except using 12 climate models participated in ISVHE and their MME mean predictions initiated from the first day of month from November to April for the 21 years of 1989-2008.

7. Summary, discussions and future direction for climate prediction

Prediction skill of Indo-Pacific climate has been rapidly improved in the past decade. While early prediction efforts were made based on statistical methods and/or simple climate models, recent climate predictions have been performed using comprehensive OAGCMs. Model performance and data assimilation scheme have been improved to produce better prediction skill. Multi-model prediction results have been collected to gain higher skill, which is usually superior to that of individual model. Most of OAGCMs now can skilfully predict MJO at lead times of up to 2-4 weeks, IOD up to 1-2 seasons, and ENSO up to 6-9 months. Distinct SST patterns associated with different El Niño flavours can also be well predicted at short-mid lead times.

Furthermore, global climate anomalies induced by ENSO and IOD can be realistically predicted. The subtropical dipole modes in the South Atlantic and IO and the southern African climate anomalies are predictable up to about one season ahead. We note that the Asian monsoon precipitation and Northern Hemisphere atmospheric circulation anomalies are also predictable at short-mid lead times (Wang et al. 2008, 2014; Lee et al. 2011). Encouragingly, the SINTEX-F model produces useful skill of ENSO prediction at lead times of up to 2 years. And some strong positive IOD events can be well predicted up to 1 year ahead even if El Niño's influence were suppressed. The results also suggest the importance of IO-Pacific inter-basin coupling and recent global warming trend to the climate predictability. There is ample space for future skill improvement of current state-of-the-art OAGCMs.

Future development of climate prediction systems includes (but not limited to):

- (i) Improving model representation of climate physics to further reduce biases in simulating mean states and climate variability (see Chapter 8 for this issue). At JAMSTEC, for instance, a second version of SINTEX-F OAGCM with high resolution and improved performance has been developed for better climate study and prediction (Masson et al. 2012; Sasaki et al. 2012a). Stratospheric processes need to be properly resolved in the model to capture the impact of stratospheric signals on the troposphere. Development of better land surface, vegetation, and sea ice models may improve regional climate prediction. Current development of Earth System Model (ESM) by including carbon cycle, atmospheric and oceanic biogeochemistry model may significantly
- improve model's representation of physical and biogeochemical processes on Earth. Although the ESM is mainly designed for climate change studies, it will also be beneficial to climate prediction since many processes resolved by the ESM also influence weather-climate time scales. Preliminary results using MPI-ESM showed encouraging skill in ENSO prediction (www.meteo.fr/cic/meetings/2013/s2d/pres/tupm_2.pdf).
- (ii) Improving data assimilation scheme in association with increasing observations. In principal, ICs of the ocean, atmosphere and other components need to be not only realistic but also balanced and compatible with model physics. Current efforts on developing coupled model data assimilation will help reduce initial shock during forecasts. Ensemble scheme needs to be improved to generate sufficient spreads to reduce the "over-confidence" problem of prediction.
- (iii) Implementing realistic external forcing into climate prediction model. Time-varying external forcing includes GHGs, aerosol, land use change, solar cycle as well as episodic volcanic eruptions. This may improve the predictions of surface temperature, precipitation, and frequency of extreme weather at seasonal-to-interannual time scales. Incorporating the external forcing also makes possible a smooth extension of seasonal-to-interannual prediction toward decadal/multidecadal prediction.
- (iv) Developing a seamless climate prediction system for intraseasonal-seasonal-interannual-decadal climate prediction. Current efforts on intraseasonal, seasonal-interannual, and decadal/multidecadal

predictions have been performed separately. However, there is no physical reason for this separation. A common notion is that intraseasonal activities may play a role in the evolution of climate signals, such as ENSO and IOD. Similarly, interannual climate variability may contribute to the decadal signals. Recent studies even suggested that climate prediction needs to be initiated from weather forecast. Accurate atmospheric ICs may improve the weather and intraseasonal prediction and hence improve climate prediction. Owing to the multi-scale interactions within the climate system, a seamless prediction system will in principal help enhance climate predictive skill.

- (v) Developing/improving seasonal prediction of the frequency of tropical cyclones (TCs). The TCs often devastate human lives and economy and hinder sustainable development of the society. Seasonal prediction of the TC frequency is possible because the TC activity is impacted by large-scale atmospheric circulation and SST anomalies induced by ENSO, IOD, MJO, Atlantic multi-decadal oscillation, etc. It was found that the North Atlantic TC frequency during June-October can be well predicted with realistic SST forcing (Vitart 2006; LaRow et al. 2008; Zhao et al. 2010) and even at multi-year timescale due to external forcing (Smith et al. 2010). Efforts have also been made on predicting the TC frequency in the Indo-Pacific area but with low skill being achieved, particularly in the IO (Alessandri et al. 2010; Takaya et al. 2010). High resolution OAGCMs with better performance in predicting large-scale climate conditions

are required to improve the skill of the TC frequency and intensity forecast. In this regard, a coupled model with ~40km resolution AGCM and ~25km resolution OGCM was developed at JAMSTEC (Sasaki et al. 2012b).

- (vi) Developing downscaling and application schemes to increase the societal value of climate prediction. Current horizontal resolution of climate prediction models is about 100-200km; this is too coarse to provide sufficiently detailed information to meet what local society requires, where the local weather and climate can be affected by small topography, frontal systems, mesoscale eddies and other subgrid-scale phenomena. Although increasing efforts have been made in last decade to develop next-generation models with ultra-high resolutions--supported by the rapid growth in computation power, making climate prediction with the next-generation model does not yet appear to be feasible in near future. Existing efforts have been focused on developing various statistical and dynamical downscaling approaches to provide better information for local areas (see Chapter 9 for one example), including probabilistic predictions of the impacts of high-risk weather-climate events. Climate prediction can also be used as external parameter in other prediction systems, such as the forest fire warning, water crisis management, health, crop yield (see Chapter 10 for one example), energy consumption prediction, etc. It has been recognized that both the quality and value of climate prediction need to be improved in future.

REFERENCES

1. Alessandri, A., A. Borrelli, S. Gualdi, E. Scoccimarro, S. Masina, 2010: Tropical cyclone count forecasting using a dynamical seasonal prediction system: Sensitivity to improved ocean initialization. *J. Climate*, **24**, 2963-2982.
2. Arribas, A., and Coauthors, 2011: The GloSea4 Ensemble Prediction System for Seasonal Forecasting. *Mon. Wea. Rev.*, **139**, 1891-1910.
3. Ashok, K., Behera, S. K., Rao, S. A., Weng, H., and Yamagata, T., 2007: El Niño Modoki and its possible teleconnection. *J. Geophys. Res.* **112**, C11007, doi:10.1029/2006JC003798.
4. Barnston, A. G., and C. F. Ropelewski, 1992: Prediction of ENSO episodes using canonical correlation analysis. *J. Climate*, **5**, 1316-1345.
5. Barnston, A. G., M. H. Glantz, and Y. He, 1999: Predictive skill of statistical and dynamical climate models in SST forecasts during the 1997-98 El Niño episode and the 1998 La Niña onset. *Bull. Amer. Meteor. Soc.*, **80**, 217-243.
6. Barnston, A. G., M. K. Tippett, M. L. L'Heureux, S. Li, and D. G. DeWitt, 2012: Skill of real-time seasonal ENSO model predictions during 2002-11. Is our capability increasing? *Bull. Amer. Meteor. Soc.*, **93**, 631-651.
7. Behera, S. K., T. Yamagata, 2001: Subtropical SST dipole events in the southern Indian Ocean. *Geophys. Res. Lett.*, **28**, 327-330.
8. Behera, S. K., J.-J. Luo, S. Masson, S. A. Rao, H. Sakuma, and T. Yamagata, 2006: A CGCM study on the interaction between IOD and ENSO. *J. Climate*, **19**, 1688-1705.
9. Bengtsson, L., U. Schlese, E. Roeckner, M. Latif, T. P. Barnett, N. Graham, 1993: A two-tiered approach to long-range climate forecasting. *Science*, **261**, 1026-1029.
10. Bessafi, M., and M. C. Wheeler, 2006: Modulation of south Indian Ocean tropical cyclones by the Madden-Julian Oscillation and convectively coupled equatorial waves. *Mon. Wea. Rev.*, **134**, 638-656.
11. Cai, M., C.-S. Shin, H. M. van den Dool, W. Wang, S. Saha, and A. Kumar, 2009: The role of long-term trend in seasonal predictions: Implications of global warming in the NCEP CFS. *Weather and Forecasting*, **24**, 965-973.
12. Cane, M. A., S. E. Zebiak, and S. C. Dolan, 1986: Experimental forecasts of El Niño. *Nature*, **321**, 827-832.
13. Chen, D., M. A. Cane, A. Kaplan, S. E. Zebiak, and D. Huang, 2004: Predictability of El Niño over the past 148 years. *Nature*, **428**, 733-736.
14. Church, J. A., N. J. White, and J. M. Arblaster, 2005: Significant decadal-scale impact of volcanic eruptions on sea level and ocean heat content. *Nature*, **438**, 74-77.
15. Dijkstra, H. A., and J. D. Neelin, 1995: Coupled ocean-atmosphere interaction and the tropical climatology. Part II: Why the cold tongue is in the east. *J. Climate*, **8**, 1343-1359.
16. Doblas-Reyes, F. J., R. Hagedorn, T. N. Palmer, and J.-J. Morcrette, 2006: Impact of increasing greenhouse gas concentrations in seasonal ensemble forecasts. *Geophys. Res. Lett.*, **33**, L07708, doi:10.1029/2005GL025061.
17. Graham, R., and Co-authors, 2011: New perspectives for GPCs, their role in the GFCS and a proposed contribution to a 'World Climate Watch'. *Clim. Res.*, **47**, 47-55, doi:0.3354/cr00963.
18. Hendon, H. H., E. Lim, G. Wang, O. Alves, and D. Hudson, 2009: Prospects for predicting two flavors of El Niño. *Geophys. Res. Lett.*, **36**, L19713, doi:10.1029/2009GL040100.
19. Hendon, H. H., and B. Liebmann, 1990: A composite study of the onset of the Australian summer monsoon. *J. Atmos. Sci.*, **48**, 2909-2923.
20. Hendon, H.H., B. Liebmann, M. Newman, J.D. Glick, and J. Schemm, 1999: [Medium range forecast errors associated with active episodes of the MJO](#). *Mon. Wea. Rev.*, **128**, 69-86.
21. Hirschi, M. et al., 2010: Observational evidence for soil-moisture impact on hot extremes in southeastern Europe. *Nature Geoscience*, **4**, 17-21.
22. Hong, C.-C., T. Li, and J.-J. Luo, 2008: Asymmetry of the Indian Ocean Dipole. Part II: Model diagnosis. *J. Climate*, **21**, 4849-4858.
23. Horii, T., H. Hase, I. Ueki, and Y. Masumoto, 2008: Oceanic precondition and evolution of the 2006 Indian Ocean dipole. *Geophys. Res. Lett.*, **35**, L03607, doi:10.1029/2007GL032464.
24. Horii, T., I. Ueki, and K. Hanawa, 2012: Breakdown of ENSO predictors in the 2000s: Decadal changes of recharge/discharge-SST phase relation and atmospheric intraseasonal forcing.

- Geophys. Res. Lett.*, **39**, L10707, doi:10.1029/2012GL051740.
25. Hsiang, S. M., K. C. Meng, and M. A. Cane, 2011: Civil conflicts are associated with the global climate. *Nature*, **476**, 438–441.
 26. Izumo, T., and Coauthors, 2010: Influence of the state of the Indian Ocean Dipole on the following year's El Niño. *Nature Geoscience* **3**, 168–172.
 27. Izumo, T. M. Lengaigne, J. Vialard, J.-J. Luo, T. Yamagata, and G. Madec, 2014: Influence of Indian Ocean Dipole and Pacific recharge on following year's El Niño: interdecadal robustness. *Clim. Dyn.*, **42**, 291–310.
 28. Jeong, H.-I., et al., 2012: Assessment of the APCC coupled MME suite in predicting the distinctive climate impacts of two flavors of ENSO during boreal winter. *Clim. Dyn.*, **39**, 475–493.
 29. Ji, M., A. Leetmaa, and V. E. Kousky, 1996: Coupled model predictions of ENSO during the 1980s and the 1990s at the National Centers for Environmental Prediction. *J. Climate*, **9**, 3105–3120.
 30. Jia, X., H. Lin, J.-Y. Lee, and B. Wang, 2012: Season-dependent forecast skill of the dominant atmospheric circulation patterns over the Pacific-North American region. *J. Climate*, **25**, 7248–7265.
 31. Jin, E. K., and Coauthors, 2008: Current status of ENSO prediction skill in coupled ocean-atmosphere models. *Clim. Dyn.*, **31**, 647–664.
 32. Jin, F.-F., 1997: An equatorial ocean recharge paradigm for ENSO. Part I: Conceptual model. *J. Atmos. Sci.*, **54**, 811–829.
 33. Kanae, S., Y. Hirabayashi, T. Yamada, and T. Oki, 2006: Influence of “Realistic” Land Surface Wetness on Predictability of Seasonal Precipitation in Boreal Summer. *J. Climate*, **19**, 1450–1460.
 34. Kataoka, T., T. Tozuka, Y. Masumoto, and T. Yamagata, 2012: The Indian Ocean subtropical dipole mode simulated in the CMIP3 models. *Clim. Dyn.*, **39**, 1385–1399.
 35. Keenlyside, N., M. Latif, M. Botzet, J. Jungclaus, and U. Schulzweida, 2005: A coupled method for initializing El Niño–Southern Oscillation forecasts using sea surface temperature. *Tellus*, **57A**, 340–356.
 36. Keenlyside, N., H. Ding, and M. Latif, 2013: Potential of equatorial Atlantic variability to enhance El Niño prediction. *Geophys. Res. Lett.*, **40**, doi:10.1002/grl.50362.
 37. Knaff, J. A., and C. W. Landsea, 1997: An El Niño Southern Oscillation climatology and persistence (CLIPER) forecasting scheme. *Weather Forecast*, **12**, 633–652.
 38. Koster, R. D., et al., 2010: Contribution of land surface initialization to subseasonal forecast skill: First results from a multi-model experiment. *Geophys. Res. Lett.*, **37**, L02402, doi:10.1029/2009GL041677.
 39. Kug, J.-S., T. Li, S.-I. An, I.-S. Kang, J.-J. Luo, S. Masson, and T. Yamagata, 2006: Role of the ENSO-Indian Ocean coupling on ENSO variability in a coupled GCM. *Geophys. Res. Lett.*, **33**, L09710, doi: 10.1029/2005GL024916.
 40. Kumar, A., and R. Murtugudde, 2013: Predictability and Uncertainty: A unified perspective to build a bridge from weather to climate. COSUST, in press.
 41. LaRow, T. E., Y.-K. Lim, D. W. Shin, E. P. Chassignet, and S. Cocks, 2008: Atlantic basin seasonal hurricane simulations, *J. Climate*, **21**, 3191–3206.
 42. Lee, J.-Y., B. Wang, I.-S. Kang, J. Shukla and Coauthors, 2010: How are seasonal prediction skills related to models' performance on mean state and annual cycle? *Clim. Dyn.*, **35**, 267–283.
 43. Lee, J.-Y., and Coauthors, 2011: How predictable is the northern hemisphere summer upper-tropospheric circulation? *Clim. Dyn.*, **37**, 1189–1203.
 44. Lee, J.-Y., B. Wang, M. C. Wheeler, X. Fu, D. E. Waliser, and I.-S. Kang, 2013: Real-time multivariate indices for the boreal summer intraseasonal oscillation over the Asian summer monsoon region. *Clim. Dyn.*, **40**, 493–509.
 45. Levitus, S. J. I. Antonov, T. P. Boyer, and C. Stephens, 2000: Warming of the World Ocean. *Science*, **287**, 2225.
 46. Liniger, M. A., H. Mathis, C. Appenzeller, and F. J. Doblas-Reyes, 2007: Realistic greenhouse gas forcing and seasonal forecasts. *Geophys. Res. Lett.*, **34**, L04705, doi:10.1029/2006GL028335.
 47. Lindesay J. A., 1988: South African rainfall, the Southern Oscillation, and a Southern Hemisphere semi-annual cycle. *J. Climate* **8**, 17–30.
 48. Lorenz, E. N., 1975: The physical bases of climate and climate modelling. *Climate Predictability*, GARP Publication Series, Vol. 16, WMO, 132–136.

49. Lorenz, D. J. and D. L. Hartmann, 2006: The effect of the MJO on the North American monsoon. *J. Climate*, **19**, 333-343.
50. Luo, J.-J., S. Masson, S. Behera, P. Delecluse, S. Gualdi, A. Navarra, and T. Yamagata, 2003: South Pacific origin of the decadal ENSO-like variation as simulated by a coupled GCM. *Geophys. Res. Lett.*, **30**, 2250, doi:10.1029/2003GL018649.
51. Luo, J.-J., S. Masson, E. Roeckner, G. Madec, and T. Yamagata, 2005a: Reducing climatology bias in an ocean-atmosphere CGCM with improved coupling physics. *J. Climate*, **18**, 2344–2360./
52. Luo, J.-J., S. Masson, S. Behera, S. Shingu, and T. Yamagata, 2005b: Seasonal climate predictability in a coupled OAGCM using a different approach for ensemble forecasts. *J. Climate*, **18**, 4474–4497.
53. Luo, J.-J., S. Masson, S. Behera, and T. Yamagata, 2007: Experimental forecasts of the Indian Ocean Dipole using a coupled OAGCM. *J. Climate*, **20**, 2178-2190.
54. Luo, J.-J., S. Masson, S. Behera, and T. Yamagata, 2008a: Extended ENSO predictions using a fully coupled ocean-atmosphere model. *J. Climate*, **21**, 84-93.
55. Luo, J.-J., S. Behera, Y. Masumoto, H. Sakuma, and T. Yamagata, 2008b: Successful prediction of the consecutive IOD in 2006 and 2007. *Geophys. Res. Lett.*, **35**, L14S02, doi:10.1029/2007GL032793.
56. Luo, J.-J., R. Zhang, S. Behera, Y. Masumoto, F.-F. Jin, R. Lukas, and T. Yamagata, 2010: Interaction between El Niño and extreme Indian Ocean Dipole. *J. Climate*, **23**, 726-742.
57. Luo, J.-J., S. Behera, Y. Masumoto, and T. Yamagata, 2011: Impact of global ocean surface warming on seasonal-to-interannual climate prediction. *J. Climate*, **24**, 1626-1646.
58. Luo, J.-J., 2011: Ocean dynamics not required? *Nature*, **477**, 544-546.
59. Luo, J.-J., W. Sasaki, and Y. Masumoto, 2012: Indian Ocean warming modulates Pacific climate change. *PNAS*, **109**, 18701-18706, www.pnas.org/cgi/doi/10.1073/pnas.1210239109.
60. Madden, R. A., and P. R. Julian, 1971: Detection of a 40-50 day oscillation in the zonal wind in the tropical Pacific. *J. Atmos. Sci.*, **28**, pp.702-708.
61. Masson, S., and Coauthors, 2005: Impact of barrier layer on winter-spring variability of the southeastern Arabian Sea. *Geophys. Res. Lett.* **32**, L07703, doi:10.1029/2004GL021980.
62. Masson, S., P. Terray, G. Madec, J.-J. Luo, T. Yamagata, and K. Takahashi, 2012: Impact of intradaily SST variability on ENSO characteristics in a coupled model. *Clim. Dyn.*, **39**, 681-707.
63. Meyers, G., P. McIntosh, L. Pigot, and M. Pook, 2007: The years of El Niño, La Niña, and interactions with the tropical Indian Ocean. *J. Climate*, **20**, 2872-2880.
64. McPhaden, M. J., 1999: Genesis and evolution of the 1997–98 El Niño. *Science*, **283**, 950–954.
65. McPhaden, M. J., X. Zhang, H. H. Hendon, and M. C. Wheeler, 2006: Large scale dynamics and MJO forcing of ENSO variability. *Geophys. Res. Lett.*, **33**, L16702, doi:10.1029/2006GL026786.
66. Meehl, G. A., J. M. Arblaster, K. Matthes, F. Sassi, and H. van Loon, 2009: Amplifying the Pacific climate system response to a small 11 year solar cycle forcing. *Science*, **325**, 1114-1118.
67. Mani, N. J., J.-Y. Lee, D. Waliser, B. Wang, and X. Jiang, 2014: Predictability of the Madden-Julian Oscillation in the Intraseasonal Hindcast Experiment (ISVHE). *J. Climate*, **27**, 4531-4543.
68. Molteni, F., and Coauthors, 2011: The new ECMWF seasonal forecast system (System 4), ECMWF Technical Memoranda, 656.
69. Moon, J.-Y., B. Wang, and K.-J. Ha, 2012: Modulation on 2009/10 winter snowstorms in the United States. *J. Climate*, **25**, 978-991.
70. Morioka, Y., T. Tozuka, T. Yamagata, 2010: Climate variability in the southern Indian Ocean as revealed by self-organizing maps. *Clim. Dyn.*, **35**, 1059-1072.
71. Morioka, Y., T. Tozuka, T. Yamagata, 2011: On the growth and decay of the subtropical dipole mode in the South Atlantic. *J. Climate*, **24**, 5538-5554.
72. Morioka, Y., T. Tozuka, S. Masson, P. Terray, J.-J. Luo, and T. Yamagata, 2012: Subtropical dipole modes simulated in a coupled general circulation model. *J. Climate*, **25**, 4029-4047.
73. Neelin, J. D., and Coauthors, 1998: ENSO theory. *J. Geophys. Res.*, **103**, 14261-14290.
74. Palmer, T. N., and Coauthors, 2004: Development of a European multimodel ensemble system for seasonal-to-interannual prediction (DEMETER). *Bull. Amer. Meteor. Soc.*, **85**, 853–872.
75. Penland, C. and L. Matrosova, 1998: Prediction of Tropical Atlantic Sea Surface Temperatures Using Linear Inverse Modeling. *J. Climate*, **11**, 483-496.

76. Rao, S. A., S. Behera, Y. Masumoto, and T. Yamagata, 2002: Interannual variability in the subsurface Indian Ocean with special emphasis on the Indian Ocean Dipole. *Deep Sea Res.*, **49**, 1549-1572.
77. Robock, A., 2000: Volcanic eruptions and climate. *Reviews in Geophysics*, **38**, 191.
78. Saha, S., and Coauthors, 2010: The NCEP Climate Forecast System Reanalysis. *Bull. Amer. Meteor. Soc.*, **91**, pp.1015-1057.
79. Saji, N. H., B. N. Goswami, P. N. Vinayachandran, and T. Yamagata, 1999: A dipole mode in the tropical Indian ocean. *Nature*, **401**, 360-363.
80. Sasaki, W., K. J. Richards, and J.-J. Luo, 2012a: Impact of vertical mixing induced by small vertical scale structures above and within the equatorial thermocline on the tropical Pacific in a CGCM. *Clim. Dyn.*, doi: 10.1007/s00382-012-1593-8.
81. Sasaki, W., J.-J. Luo, and S. Masson, 2012b: Tropical cyclone simulation in a high-resolution atmosphere-ocean coupled general circulation model. "Cyclones: Formation, triggers and control" edited by K. Oouchi and H. Fudeyasu, NOVA publishers, New York.
82. Shi, L., H. H. Hendon, S. Alves, J.-J. Luo, M. Balmaseda, and D. Anderson, 2012: How predictable is the Indian Ocean Dipole? *Mon. Wea. Rev.*, **140**, 3867-3884.
83. Sigmond, M., J. F. Scinocca, V. V. Kharin and T. G. Shepherd, 2013: Enhanced seasonal forecast skill following stratospheric sudden warmings. *Nature Geoscience*, doi: 10.1038/NGEO1698.
84. Smith, D. M., R. Eade, N. J. Dunstone, D. Fereday, J. M. Murphy, H. Pohlmann, A. Scaife, 2010: Skilful multi-year predictions of Atlantic hurricane frequency. *Nature Geoscience*, **3**, 846-849.
85. Sperber, K. R., S. Gualdi, S. Legutke, and V. Gayler, 2005: The Madden-Julian oscillation in ECHAM4 coupled and uncoupled general circulation models. *Clim. Dyn.*, **25**, 117-140.
86. Sperber, K. R., and D. E. Waliser, 2008: New Approaches to Understanding, Simulating, and Forecasting the Madden-Julian Oscillation. *Bull. Am. Meteor. Soc.*, doi: 10.1175/2008BAMS2700.1.
87. Stockdale, T. N., M. A. Balmaseda, A. Vidard, 2006: Tropical Atlantic SST prediction with coupled ocean-atmosphere GCMs. *J. Clim.*, **19**, 6047-6061.
88. Stockdale, T. N., and Colleagues, 2010: Understanding and Predicting Seasonal-to-Interannual Climate Variability - The Producer Perspective. *Procedia Environmental Sciences* **1**, 55-80.
89. Takaya, Y., T. Yasuda, T. Ose, and T. Nakaegawa, 2010: Predictability of the mean location of typhoon formation in a seasonal prediction experiment with a coupled general circulation model, *J. Meteor. Soc. Japan*, **88**, 799-812.
90. van den Dool, H. M., J. Huang, and Y. Fan, 2003: Performance and analysis of the constructed analogue method applied to U.S. soil moisture over 1981-2001. *J. Geophys. Res.*, **108**, D16, 8617, doi:10.1029/2002JD003114.
91. Venegas, S.A., L. A. Mysak, and D. N. Straub, 1997: Atmosphere-ocean coupled variability in the South Atlantic. *J. Climate*, **10**, 2904-2920.
92. Vigaud, N., Y. Richard, M. Rouault, and N. Fauchereau, 2009: Moisture transport between the South Atlantic Ocean and southern Africa: relationships with summer rainfall and associated dynamics. *Clim. Dyn.*, **32**, 113-123.
93. Vitart, F., 2006: Seasonal forecasting of tropical storm frequency using a multi-model ensemble, *Q. J. R. Meteorol. Soc.*, **132**, 647-666.
94. Wajswicz, R. C., Wajswicz, R. C., 2005: Potential predictability of tropical Indian Ocean SST anomalies. *Geophys. Res. Lett.*, **32**, L24702, doi:10.1029/2005GL024169.
95. Wang, B., and Coauthors, 2005: Fundamental challenge in simulation and prediction of summer monsoon rainfall. *Geophys. Res. Lett.*, **32**, L15711.
96. Wang, Bin, June-Yi Lee, I.-S. Kang, J. Shukla, J.-S. Kug, A. Kumar, J. Schemm, J.-J. Luo, T. Yamagata, and C.-K. Park, 2008: How accurately do coupled climate models predict the leading modes of Asian-Australian monsoon interannual variability? *Clim. Dyn.*, **30**, 605-619.
97. Wang, B., and Coauthors, 2009: Advance and prospectus of seasonal prediction: assessment of the APCC/CliPAS 14-model ensemble retrospective seasonal prediction (1980-2004). *Clim. Dyn.*, **33**, 93-117.
98. Wang, B., June-Yi Lee, and Baoqiang Xiang, 2014: Asian summer monsoon rainfall predictability: A predictable mode analysis. *Clim. Dyn.* in press, doi:10.1007/s00382-014-2218-1.

99. Wheeler, M. C., and H. H. Hendon, 2004: An All-Season Real-Time Multivariate MJO Index: Development of an Index for Monitoring and Prediction. *Mon. Wea. Rev.*, **132**, 1917-1932.
100. Wu, A., W. W. Hsieh and B. Tang, 2006: Neural network forecasts of the tropical Pacific sea surface temperatures. *Neural Networks*, **19**, 145-154.
101. Xie, S.-P., H. Annamalai, F. A. Schott, and J. P. McCreary, 2002: Origin and predictability of South Indian Ocean climate variability. *J. Climate*, **15**, 864-874.
102. Xue, Y., A. Leetmaa, and M. Ji, 2000: ENSO prediction with Markov models: The impact of sea level. *J. Climate*, **13**, 849-871.
103. Xue, Y., and Co-authors, 2011: An Assessment of Oceanic Variability in the NCEP Climate Forecast System Reanalysis. *Clim. Dyn.*, **37**, 2511-2539, doi:10.1007/s00382-010-0954-4.
104. Yamagata, T., S. Behera, J.-J. Luo, S. Masson, M. Jury, and S. A. Rao, 2004: Coupled ocean-atmosphere variability in the tropical Indian Ocean. *Earth's Climate: The Ocean-Atmosphere Interaction. Geophys. Monogr.* **147**, Amer. Geophys. Union, 189-212.
105. Yuan, C., T. Tozuka, J.-J. Luo, T. Yamagata, 2014a: Predictability of the subtropical dipole modes in a coupled ocean-atmosphere model. *Clim. Dyn.*, **42**, 1291-1308.
106. Yuan, C., T. Tozuka, W. A. Landman, T. Yamagata, 2014b: Dynamical seasonal forecast of the southern African summer precipitation. *Clim. Dyn.*, **42**, 3357-3374.
107. Zhang, C., and Coauthors, 2013: Cracking the MJO nut. *Geophys. Res. Lett.*, **40**, 1123-1230.
108. Zhao, M., I. M. Held, and G. A. Vecchi, 2010: Retrospective forecasts of the hurricane season using a global atmospheric model assuming persistence of SST anomalies. *Mon. Wea. Rev.*, **138**, 3858-3868.